OPTICAL MICROMANIPULATION USING DISPERSION-COMPENSATED AND PHASE-SHAPED ULTRASHORT PULSED LASERS

Janelle Shane

A Thesis Submitted for the Degree of MPhil
at the
University of St. Andrews

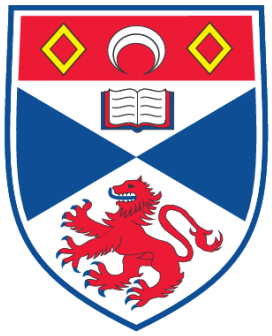

2009

Optical micromanipulation using dispersion-compensated and phase-shaped ultrashort pulsed lasers

Janelle Shane

Thesis for the degree of Masters of Philosophy

School of Physics and Astronomy

University of St Andrews

St Andrews, Fife, Scotland

Submitted 8 January, 2009

I, Janelle Claire Shane, hereby certify that this thesis, which is approximately 24,000 words in length, has been written by me, that it is the record of work carried out by me and that it has not been submitted in any previous application for a higher degree.

Date 9.5.09 Signature of Candidate

I was admitted as a research student in August 2007 and as a candidate for the degree of Master of Philosophy in August 2007; the higher study for which this is a record was carried out in the University of St Andrews between 2007 and 2008.

Date 9.5.09 Signature of Candidate

I hereby certify that the candidate has fulfilled the conditions of the Resolution and Regulations appropriate for the degree of Master of Philosophy in the University of St Andrews and that the candidate is qualified to submit this thesis in application for that degree.

Date 19.5.09 Signature of Supervisor

In submitting this thesis to the University of St Andrews we understand that we are giving permission for it to be made available for use in accordance with the regulations of the University Library for the time being in force, subject to any copyright vested in the work not being affected thereby. We also understand that the title and the abstract will be published, and that a copy of the work may be made and supplied to any bona fide library or research worker, that my thesis will be electronically accessible for personal or research use unless exempt by award of an embargo as requested below, and that the library has the right to migrate my thesis into new electronic forms as required to ensure continued access to the thesis. We have obtained any third-party copyright permissions that may be required in order to allow such access and migration, or have requested the appropriate embargo below.

The following is an agreed request by candidate and supervisor regarding the electronic publication of this thesis:

Access to Printed copy and electronic publication of thesis through the University of St Andrews.

Date 7.7.08 Signature of candidate

Date 18.5.09 Signature of supervisor

Abstract

Ultrashort pulsed lasers offer high peak powers at low average powers, making them ideal for maximising the efficiency of nonlinear excitation. Their broad bandwidths make it possible to tailor the pulse's temporal profile for advanced control of multiphoton excitation, techniques known as pulse shaping. This thesis represents the first combination of ultrashort pulse shaping with optical trapping and axicon dispersion compensation.

We construct an optical trapping system which incorporates a 12fs duration pulsed laser, the shortest duration used to date in optical trapping. To achieve 12fs pulse durations at the sample, we must first eliminate temporal dispersion, which stretches and distorts pulses as they travel through microscope systems. We use the Multiphoton Intrapulse Interference Phase Scan (MIIPS) method to measure and compensate all orders of dispersion in our optical trapping system, verifying 12-13fs pulses at the sample.

We use the dispersion-compensated optical trapping system to investigate the effects of pulse duration on optical trapping. Our theoretical arguments show that trap stiffness is independent of pulse duration. For experimental verification, we measure the trap stiffness of trapped 780nm silica spheres with back focal plane interferometry as we change pulse duration by more than an order of magnitude using quadratic pulse shaping. We find the trap stiffness unchanged within 9%.

We also use quadratic pulse shaping to control two-photon fluorescence in optically trapped fluorescent polymer spheres. Next, we demonstrate two methods for producing selective two-photon excitation in trapped particles: amplitude shaping and 3rd order pulse shaping.

Finally, we compensate dispersion in an axicon system, producing a non-diffracting ultrashort Bessel beam with controllable dispersion. This forms

the basis for ongoing experiments exploring ultrashort Bessel beams in cellular transfection (photoporation), and examining the spatial profile of the Bessel beam as a function of the pulse's temporal profile.

Contents

Abbreviations

CW	continuous-wave
FWHM	full width at half maximum
CARS	coherent anti-Stokes Raman scattering
NA	numerical aperture
MIIPS	multiphoton intrapulse interference phase scan
TL	transform-limited
GVD	group velocity dispersion
SLM	spatial light modulator
SHG	second harmonic generation
FROG	frequency-resolved optical gating
SPIDER	spectral shear interferometry for direct electric field reconstruction
QPD	quadrant photodiode
KDP	potassium dihydrogen phosphate (KH_2PO_4)
BBO	beta barium borate (beta-BaB_2O_4)
MDU	microscope detection unit
KTP	potassium titanium oxide phosphate ($KTiOPO_4$)
LMPC	laser microdissection and pressure catapulting

Table 1:
Abbreviations used in this thesis

Chapter 1

Introduction

1.1 Motivation: ultrashort pulses in optical micromanipulation and laser ablation

1.1.1 Optical micromanipulation

Optical micromanipulation, a diverse set of techniques involving the use of light to move microscopic objects, has led to advances in a wide array of areas. One popular form of optical micromanipulation is optical trapping[1], in which a highly focused beam of light is used to hold or move objects in two or three dimensions with precisely calibrated forces, or to cool trapped matter for use in studies of Bose-Einstein condensates[2]. Trapped particles can be used as probes to measure the forces exerted by motor proteins[3] or to measure the characteristics of a nearby surface or particles[4]. Optical micromanipulation allows study and/or sorting of single trapped particles, or of hundreds of particles in precisely-specified configurations[5].

Optical micromanipulation primarily depends on linear physical properties of materials, so continuous-wave (CW) lasers are usually the sources used for optical trapping. However, researchers are increasingly using pulsed lasers instead of or in addition to CW sources, seeking to employ nonlinear effects in

combination with optical trapping. Pulsed lasers offer extremely high peak powers at lower average powers, and therefore allow access to new multiphoton processes that would otherwise require enormously high average powers. Nonlinear effects that have been combined with optical trapping include two-photon excitation[6, 7], second harmonic generation[8, 9], multiphoton ablation and self-focusing[10], coherent anti-Stokes Raman scattering[11], and two-photon morphology-dependent resonances[12, 13].

It would be useful to be able to carry out these studies using not only Gaussian beams, but also more advanced light fields. Holographic traps, for example, allow the study of hundreds of trapped particles in highly-reconfigurable 2D or 3D geometries[5]. Bessel beams, another type of advanced light field, offers long guiding distances[14] and self-reconstructs around obstacles[15]. The use of ultrashort pulses for optical trapping using these light fields has remained unexplored.

1.1.2 Laser ablation

In addition to moving microscopic objects, light can also be used to cut them very precisely. Controlled ablation has found clinical and industrial use on the macroscopic scale, in laser eye surgery and industrial machining. The technique has been used on the microscopic scale as well, for example, for cutting chromosomes[16].

One major microscopic application of laser ablation is photoporation, a technique in which a laser is used to machine an extremely small temporary hole in the lipid bilayer of cellular membranes. Through this hole, substances such as DNA or drugs can be introduced[17], after which the membrane heals the hole, restoring cellular integrity. In this way, cellular transfection or drug delivery can be performed on individual cells which can then be tracked and monitored. In poration it is important to minimise damage to surrounding areas of the cell membrane if the cell is to be able to repair the hole and survive. Photoporation offers several advantages over other methods of cellular transfection, including

its compatibility with modern microscope systems, high efficiency, non-contact operation, and ability to individually address cells.

Pulsed lasers are often used for laser ablation, due to their high peak powers, allowing highly-efficient multiphoton laser ablation at low average powers. Multiphoton excitation is highly localised at the laser focus, so multiphoton laser ablation can produce smaller, cleaner holes than single-photon ablation[18]. The lower average powers required mean that thermal effects such as melting are minimised. These advantages have been put to use in many techniques involving pulsed laser ablation of biological tissue[18]. Cellular transfection performed by pulsed laser photoporation can have a very high efficiency and cell survival rate[19]. The use of ultrashort laser pulses should allow the use of even lower average powers, further increasing cellular viability[20].

1.1.3 Ultrashort lasers and pulse shaping

The ratio of peak power to average power, and therefore the efficiency of multiphoton excitation, is inversely related to pulse duration. These effects become dramatic as pulse duration drops below 50fs (Figure 1.1); however, the exploitation of varying pulse durations in optical micromanipulation has remained almost completely unexplored.

This thesis will focus on the use of ultrashort pulsed lasers in optical trapping, with brief discussion of applications in Bessel beam photoporation. Definitions of "ultrashort" differ, but the term here refers to durations below 50fs full width at half maximum (FWHM), in contrast to the 100fs and longer durations more commonly used. At these durations, the laser's bandwidth increases from a few nanometres to tens or even hundreds of nanometres, and begins to play a very noticeable role in the way the laser interacts with materials. Peak power also increases dramatically compared to a 100fs pulse at the same average power, becoming orders of magnitude higher (Figure 1.1). Multiphoton effects such as two-photon excitation and second harmonic generation therefore greatly increase in efficiency, allowing lower average powers to be used. Accordingly,

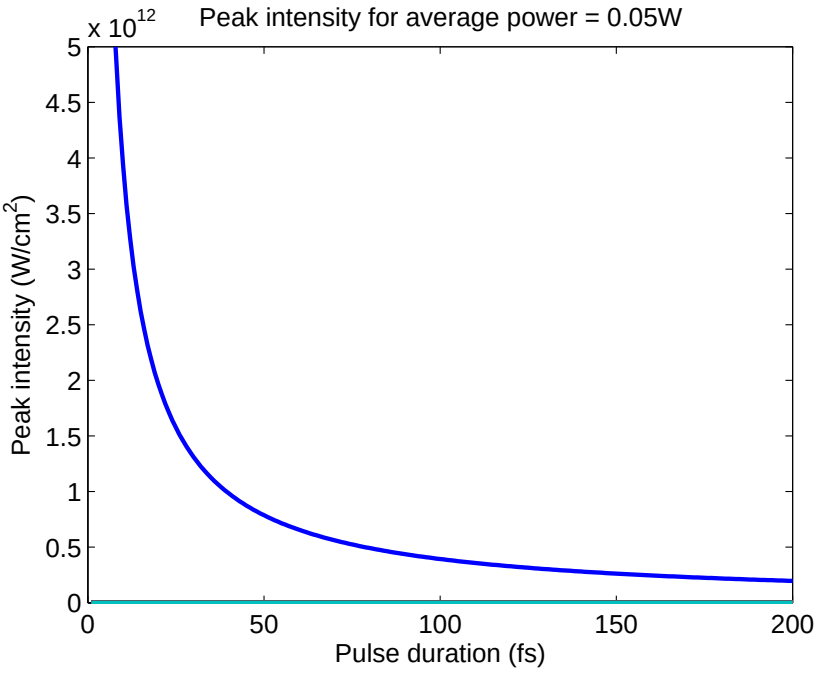

Figure 1.1:
Peak intensity vs pulse duration for an 80MHz pulsed laser source of 50mW average power, focused to a spot of 1.1μm diameter.

detrimental effects such as photobleaching and thermal damage are reduced[21].

The broad bandwidths of ultrashort pulses have enabled a new and rapidly-growing area of nonlinear excitation, known as pulse shaping. In these techniques ultrashort lasers, with carefully-controlled spectral phase across their broad bandwidths, are used to produce highly-selective nonlinear effects. The number of applications of pulse shaping is quickly increasing, driven in part by the increasing availability of reliable, compact, and low-cost ultrashort lasers. To date, pulse shaping has been used for applications such as low-background single-beam coherent anti-Stokes Raman Scattering (CARS)[22], highly accurate refractive index measurement[23, 24], precise measurement of two-photon excitation spectra[25], and selective multiphoton excitation without wavelength tuning or filters[26].

This thesis represents a combination of recent advances in pulse shaping with the selectivity and flexibility of optical micromanipulation and laser ablation. These experiments are the first instance of optical trapping with ultrashort pulses, as well as the first experimental investigation of optical trapping forces as a function of pulse duration, and the first demonstration of pulse shaping to control nonlinear processes in optically trapped particles. In addition, a system is developed that would allow the use of ultrashort pulsed Bessel beams for cellular transfection, and other studies. As explained below, none of these experiments would be possible without first applying a major recent development in pulse shaping, the ability to measure and compensate for all orders of dispersion within a high numerical aperture microscope system.

1.2 Dispersion: mortal enemy of the ultrashort laser pulse

Despite their advantages of increased peak power and bandwidth, ultrashort ($<$50fs) pulses have not been used in optical trapping to date. The reason is not the availability of ultrashort lasers – turnkey systems with durations below

50fs have been commercially available for years. Currently, it is possible to buy ultrashort pulsed lasers with durations as low as 10fs. The price of these systems has been decreasing, and their reliability increasing. A primary reason these lasers have not found widespread use is the problem of temporal dispersion. [1]Temporal dispersion is an effect by which ultrashort pulses are stretched as they travel through microscope systems, particularly through high numerical aperture (NA) objectives. By the time they reach the sample, ultrashort pulses can be stretched by orders of magnitude, with peak power (and therefore multiphoton excitation efficiency) accordingly reduced. This happens because of the broadband nature of an ultrashort light pulse – the speed of light in materials is wavelength dependent, so some wavelengths travel faster through the microscope system than others. This creates a time lapse between the arrival of the faster and the slower wavelengths, lengthening the pulse and changing the spectrum the sample sees as a function of time. The effect is extremely pronounced for microscope systems, which have a large amount of dispersive material.

The dispersion in an optical system, if precisely known, can be compensated for by manually pre-dispersing the laser pulses with the opposite dispersion, so the net dispersion at the sample is zero. Measuring and compensating dispersion is not straightforward, due to the extremely short timescales involved and the complex wavelength dependence of refractive index for the various materials and coatings within an optical system. The problem is compounded for microscope systems, due to geometrical restrictions and the magnitude and complexity of dispersion these systems introduce. Only recently has it been possible to completely compensate for all orders of dispersion compensation in a microscope system. This thesis demonstrates the first incorporation of the MIIPS (Multiphoton Intrapulse Interference Phase Scan) dispersion measurement and compensation method into an optical trapping system. In addition, the MIIPS method is used to compensate dispersion in an ultrashort Bessel beam created by an axicon, with the aim of Bessel beam photoporation.

[1]Although spatial dispersion is also a factor due to the large bandwidth of these pulses, it is less of a problem and correctable using apochromatic optics [27], and is not discussed here.

1.3 Organisation of this thesis

The body of this thesis is divided into 6 chapters.

- Chapter 2 will discuss the problem of temporal dispersion of ultrashort pulses in microscope systems. The chapter will present some current methods of measuring and/or compensating for dispersion.

- Chapter 3 describes the construction of an optical trapping system and a Bessel beam photoporation system, and the incorporation of the MIIPS dispersion measurement and compensation into these systems. Experimental results demonstrate successful dispersion compensation.

- Chapter 4 contains a theoretical and experimental investigation of optical trapping as a function of pulse duration, and a first demonstration of control of nonlinear excitation in trapped particles through pulse shaping.

- Chapter 5 describes the development and dispersion compensation of an axicon-containing microscope system. This system is being used in ongoing work on Bessel beam photoporation and studies of ultrashort Bessel beam spatial profile as a function of temporal profile.

- Chapter 6 summarises and concludes the thesis.

Chapter 2

Dispersion measurement and compensation in microscope systems

2.1 Introduction

2.1.1 What is temporal dispersion?

Although ultrashort (<50fs) pulsed laser systems have been available for decades, there has been little or no work with them in optical trapping or photoporation. One primary reason for this is the problem of temporal dispersion, which is particularly acute for the high numerical aperture (NA) microscope systems needed for these applications. The characteristic that makes ultrashort pulses so susceptible to temporal dispersion (for reasons discussed below) is their broadband nature. The frequency bandwidth of a pulsed laser source is related to its time bandwidth via the uncertainty principle. The shorter the pulse, the broader its bandwidth. The minimum pulse duration possible for a Gaussian pulse of given

bandwidth can be calculated using the relation[28]

$$\Delta t = \frac{0.44}{\Delta \nu} \tag{2.1}$$

where Δt is the full width at half maximum (FWHM) time duration, and $\Delta \nu$ is the minimum FWHM frequency duration of the pulse. The factor in the numerator depends on the shape of the pulse and is called the time-bandwidth product of the pulse; this value is 0.44 for a Gaussian pulse and 0.315 for a sech^2 pulse. A pulse that has the minimum attainable frequency is said to be transform-limited (TL). Figure 2.1 shows the calculated TL pulse duration for a Gaussian pulse centred at 800nm, for a range of FWHM wavelength bandwidths. As is evident from this image, once pulse duration drops below 30fs or so, a small decrease in pulse duration will produce a dramatic increase in bandwidth (and therefore a dramatic increase in dispersion, as will be discussed below). The broad bandwidth of an ultrashort laser pulse can offer advantages, such as the excitation of a broader range of fluorescent dyes, or the simultaneous pumping of two energy levels. A broad bandwidth also allows the possibility of controlling the phase and amplitude of different wavelength ranges within the pulse, to produce a custom-tailored pulse for a particular process. However, this broad bandwidth also causes dispersion problems.

In a TL pulse, all wavelengths arrive at the sample at the same time. However, dispersive effects, which occur when a pulse travels through a medium such as glass, water, or even air, can cause some wavelengths within the pulse to arrive later than others. This is due to the wavelength dependence of refractive index within materials. The speed of a given wavelength of light within a medium can be calculated using the refractive index of the medium at that wavelength, $n_{mat}(\lambda)$, according to Equation 2.2,

$$\nu(\lambda) = \frac{c}{n_{mat}(\lambda)} \tag{2.2}$$

where $\nu(\lambda)$ is the speed of light in the medium and c is the speed of light in

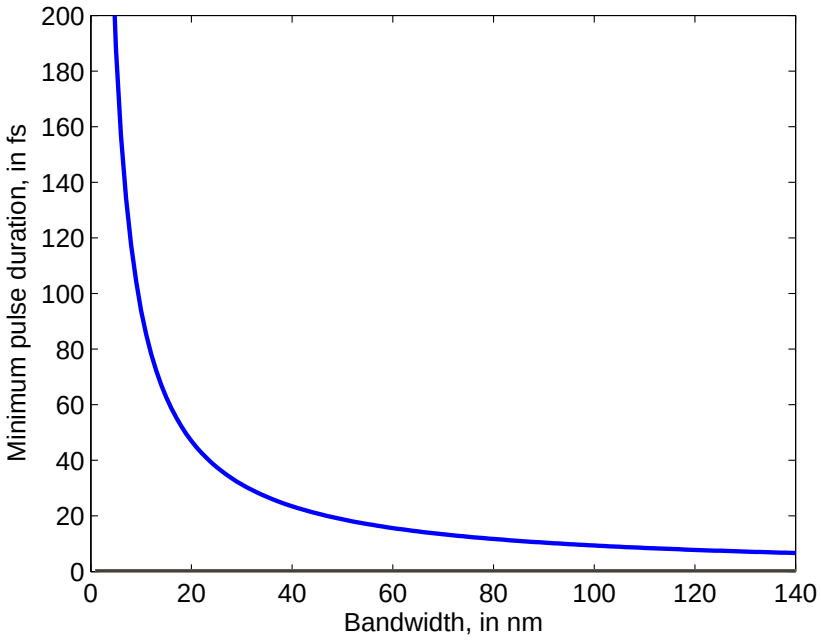

Figure 2.1:
Calculated minimum pulse duration (TL pulse duration) of a Gaussian pulse centred at 800nm, for given FWHM wavelength bandwidths.

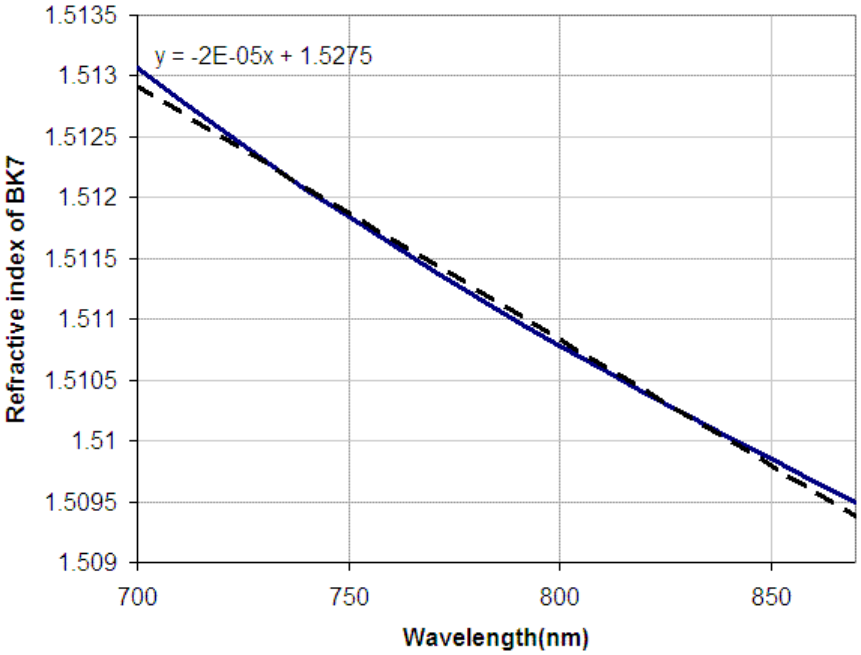

Figure 2.2:
Solid line: refractive index of BK7 glass as a function of wavelength. Dashed line: linear fit to the refractive index data ($y = (-2.5E-5)x + 1.5275$). Notice the deviation of the refractive index data from a linear relationship; this indicates the presence of 3rd order and higher dispersive effects. (Data from [29])

a vacuum. A difference in refractive index between two wavelengths in a given material corresponds to a difference in the speed at which each wavelength travels as it passes through the medium. Figure 2.2 shows the wavelength dependence of refractive index for BK7 glass (blue curve) over the wavelength region 700-870nm (the wavelength range covered by the 12fs source used in this work)[29]. A linear fit is included for reference (dashed line); note that the refractive index largely follows a linear function of wavelength, but also has some higher-order deviations from linearity. These deviations become very noticeable when working with ultrashort pulses, as will be discussed later.

The effect of this wavelength dependence is that some wavelengths within a broadband ultrashort pulse travel slightly slower than others when they go through lenses, microscope objectives, dielectric mirror coatings, coverslips,

and other media. By the time the pulse reaches the sample, the faster wavelengths are significantly ahead of the slower wavelengths, and the pulse appears "chirped". (The term "chirp" to refer to a short burst of light with different arrival times for different frequencies comes from an analogy to sound, where a "chirp" sound is characterised by a short duration with a quick change from low to high frequencies.) The net effect of this dispersion is a lengthening of the pulse at the sample, and an often complex frequency vs arrival time dependence.

Dispersion of ultrashort pulses is often discussed in terms of spectral phase. In a TL pulse, all wavelengths are in phase with each other. Slowing some wavelengths is equivalent to applying a phase delay to these wavelengths, so they arrive behind (that is, out of phase with) the other wavelengths. Knowing the refractive index as a function of wavelength (as in Figure 2.2), and the amount of medium that the pulse travels through, we can calculate the total phase delay as a function of wavelength (the laser pulse's spectral phase). For BK7 glass, this function is roughly quadratic (due to the refractive index vs wavelength relation being mostly linear), and dispersion is dominated by 2^{nd} order dispersion, often called group velocity dispersion (GVD). However, there are also 3^{rd} order and higher phase delays that play an increasingly significant role as bandwidth increases. Anti-reflection coatings and dielectric mirrors tend to introduce a particularly large amount of higher order distortions.

Although dispersive effects on 100fs and longer pulses are relatively subtle, even for microscope systems with plenty of glass and coatings, they become very significant for shorter pulses. This is due to the increased bandwidth of ultrashort pulses. Over a short wavelength range, the refractive index of most materials does not change very much, so there is not much difference between the arrival times of the fastest and slowest wavelengths within the narrow bandwidth (see Figure 2.1) of a 100fs pulse. However, a broadband ultrashort pulse can be dramatically stretched. In a typical microscope system, for example, a pulse that was originally 12fs can end up orders of magnitude longer at the sample than a pulse that was originally 120fs. This is illustrated by Figure 2.3, which

shows the final durations of pulses with different initial durations, after travelling through a typical microscope system. Figure 2.3 was calculated using

$$\tau_f = \tau_i \sqrt{1 + \frac{16 \log(2)^2 \phi_2^2}{\tau_i^2}} \tag{2.3}$$

where τ_f is the final FWHM (full width at half maximum) pulse duration, τ_i is the initial FWHM pulse duration, and ϕ_2 is the total 2nd order dispersion[30]. The total 2nd order dispersion ϕ_2 can be calculated for a given amount of material if the $n(\lambda)$ is known for the material:

$$\phi_2 = \frac{\lambda_0^3 c^2 n"(\lambda) l}{2\pi} \tag{2.4}$$

where λ_0 is the wavelength of interest, c is the speed of light, $n"(\lambda)$ is the 2nd derivative of the refractive index with respect to λ, and l is the length of the material through which the pulse travels[30]. Figure 2.3 uses a ϕ_2 of 7000 fs^2, a typical figure for a microscope system with a high NA objective[27].

Note that in the calculations for Figure 2.3, only 2nd order distortions are taken into account. Microscope systems also have significant higher-order dispersion that further lengthens the pulse, as well as changing its temporal shape. By the time they reach the sample, the pulses no longer have a Gaussian time profile, so FWHM pulse duration becomes a less meaningful measure of how much a pulse has been stretched. In this thesis I will refer to the pulse durations of uncompensated pulses for convenience, but these numbers should be taken only as a rough indication of how much the pulses are stretched. FWHM pulse duration is still a relevant measure for TL pulses and for pulses only stretched by 2nd order distortions.

As the above discussion shows, the effects of dispersion are major obstacles that must be overcome if ultrashort pulses are to be used in microscope systems. Most strategies seek to measure or estimate the total dispersion in the system, then apply the opposite dispersion to the pulses so that the total dispersion is zero at the sample plane. This general approach is called dispersion

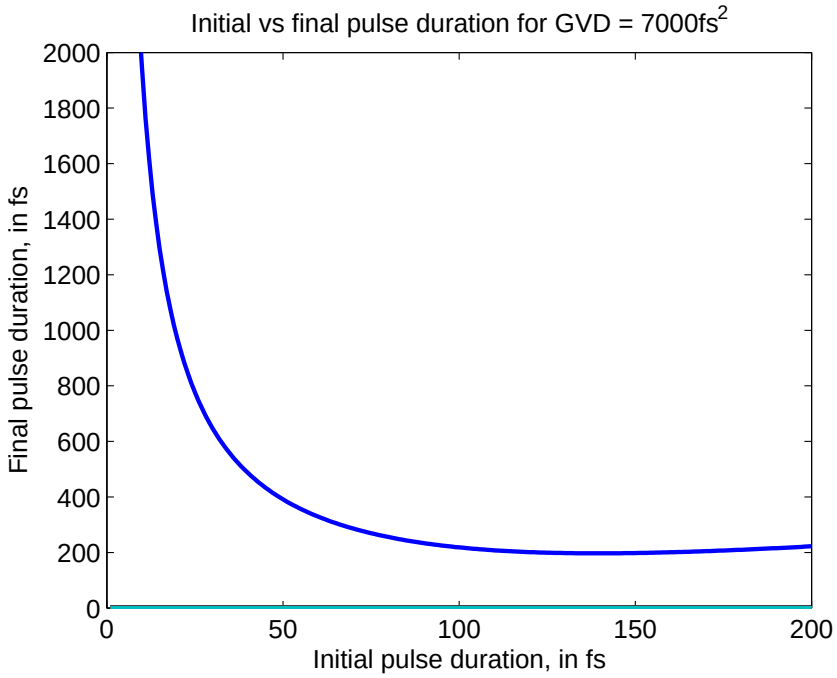

Figure 2.3:
Calculated effect of dispersion on the FWHM duration of ultrashort pulses travelling through a typical microscope system. Here, the amount of dispersion is 7000fs^2, a typical amount for a microscope system with high NA objective[27]. This calculation only considers GVD (2nd order distortions); microscope systems also have significant higher-order dispersion that further lengthens the pulse, as well as changing its temporal shape (making FWHM pulse duration less meaningful).

pre-compensation. Much of the challenge in dispersion pre-compensation lies in measuring the dispersion that must be compensated, with higher-order dispersion posing particular difficulty. The following sections will discuss some of the major methods for: 1) pre-compensating dispersion in microscope systems, 2) measuring dispersion in microscope systems, and 3) combined dispersion measurement and pre-compensation in microscope systems.

2.2 Dispersion pre-compensation

This section describes some of the most widely-used methods for dispersion pre-compensation in microscope systems. The methods discussed in this section do not measure dispersion, although some can be used to provide rough estimates of 2nd order dispersion, or as part of an algorithm that measures and compensates dispersion.

2.2.1 Prism/grating pre-compressor

In use since the earliest days of pulsed lasers, the method of pulse pre-compression by prism[31] or grating[32] pair is one of the oldest, simplest, and cheapest methods to pre-compensate dispersion. In the prism version of this method, four prisms are used to spread, propagate, and recombine the wavelengths within a pulse in such a way that there is a path length difference between the longest and shortest wavelengths in the pulse. This creates negative group velocity dispersion (GVD), in other words, the negative 2nd order dispersion needed to overcome the large amounts of positive 2nd order dispersion introduced by the glass in a microscope system (Figure 2.4). With a similar geometry, gratings can also be used as the dispersive elements. By adjusting the distance between the prisms or gratings, the amount of negative 2nd order dispersion can be adjusted. Usually two prisms or gratings are used along with a folding mirror instead of four prisms or gratings, as shown in Figure 2.4. A single-prism design has also been recently demonstrated[33].

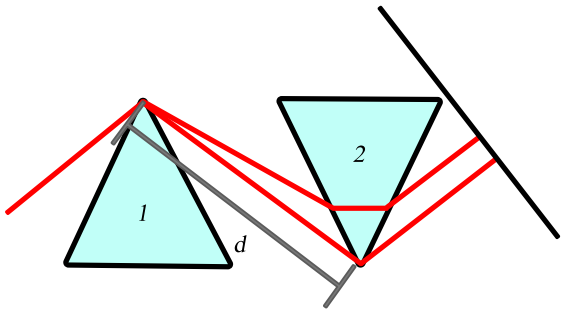

Figure 2.4:
Four-prism pre-compressor, folded into a two-prism design using a mirror (Figure adapted from [31]). The amount of negative 2nd order dispersion introduced depends on the length d between prism pairs. Prism 1 spreads the beam into constituent frequencies, which separate from each other as they propagate the distance d. Prism 2 collects and collimates the spread beam, sending it to the folding mirror. The folding mirror sends the spread beam back to Prism 2, which recollects the beam's frequencies into a single collinear beam at Prism 1, at which point the beam exits from the prism system (usually a slight height difference is introduced into the beam so the output beam can be picked off).

The choice of prism versus grating depends primarily on efficiency/table space requirements. Gratings cause significant power losses due to higher-order diffraction, so prisms are often chosen when power transmission needs to be maximised. On the other hand, prisms are not as dispersive as gratings, so a prism pre-compressor requires a much longer path length than an equivalent grating pre-compressor. The beam spreads as it travels between the prism tips, so at large prism separations the beam can reach centimetres in length by the time it reaches the second prism, meaning that the second prism often has to be very large so that clipping does not occur. A prism compressor can be made more compact by using highly dispersive glass such as SF10 or ZF4.

Note that the prism/grating pre-compressor does not measure dispersion. By iteratively changing the prism/grating distances and checking pulse duration via a method such as autocorrelation, a prism/grating distance that produces minimum pulse duration (and therefore the best dispersion compensation) can be found. From the measured prism/grating distances, it is possible to estimate the amount of dispersion that was compensated. For a prism compressor, the

accuracy of this estimate depends on being able to know the precise amount of prism material the pulse travels through, a number that is difficult to measure accurately.

The prism/grating compressor only compensates 2nd order dispersion and in fact introduces significant higher-order dispersion, one of the primary disadvantages of this kind of dispersion compensation. With 2nd order dispersion compensation only, combined with the introduced higher-order dispersion, it has been calculated that it is not possible to achieve pulses with less than 30fs pulse duration at the sample plane of a high-NA microscope, no matter how short the starting duration [27].

When absolute minimum pulse duration is not required, and small day-to-day variations in higher-order dispersion can be tolerated, the prism/grating pre-compressor is an attractive option. Since higher-order dispersion is not as detrimental to narrow-bandwidth pulses, this technique is often used to compress pulses with longer TL durations.

One primary advantage of the grating/prism precompressor is that it provides relatively simple and inexpensive compensation of large amounts of 2nd order dispersion, in quantities which many other dispersion compensation techniques cannot achieve due to hardware limitations. Grating/prism precompressors are therefore often used in combination with other dispersion compensation techniques.

2.2.2 Chirped mirror pre-compressor

The chirped mirror pre-compressor[34] is similar in many ways to the prism/grating pre-compressor. This type of pre-compressor also compensates rather than measures dispersion, and can be placed at any point in the beam path. Chirped mirrors are fabricated with dielectric coatings that are specially-tailored to impart specific phase delays to each wavelength reflecting off of the mirror. Often chirped mirrors are used in pairs so that their effects can be magnified via multiple bounces. In dispersion pre-compensating chirped mirrors, the mirrors are

designed to produce negative GVD with each bounce (thus compensating for some of the positive 2nd order dispersion that the pulse will accumulate in the rest of the optical system). Chirped mirrors can additionally be designed to minimise the 3rd and higher order distortions they impart, or to provide a certain amount of higher-order dispersion compensation with each bounce. Chirped mirror pre-compressors can be made very compact, and advanced designs can have extremely low loss, as well as operate over large bandwidths[35].

The amount of dispersion introduced by a pair of chirped mirrors can be coarsely controlled by adjusting the number of times the beam bounces between the mirrors. The number of possible bounces is limited by geometry, placing an upper limit on the amount of dispersion that can be compensated with a given pair of chirped mirrors. To increase this range, chirped mirrors can be designed that produce larger amounts of dispersion compensation with each bounce. However, this makes the dispersion adjustment coarser, and these mirrors may operate over a smaller bandwidth than other chirped mirrors[36].

Although chirped mirrors, unlike prism/grating precompressors, can simultaneously compensate 2nd order and higher order dispersion, they impart a fixed amount of this dispersion-compensating phase delay per bounce, so they are able only to compensate highly-specific dispersion functions. Thus, to adapt to the change in dispersion caused by the insertion of extra beam expanders, polarisers, coated mirrors, or in particular, different microscope objectives, chirped mirror pairs must be added and/or replaced.

Despite their limited flexibility, chirped mirror pairs can be designed to accurately and totally eliminate the dispersion (if known) in a given optical system. Chirped mirrors are widely used in cancelling dispersion within the cavities of ultrashort pulsed lasers, where the dispersion is known and roughly constant. They have also been used in combination with a prism pre-compressor to compensate for most of the dispersion of microscope systems (the most complete compensation was achieved for lower-NA microscope objectives)[37]. This application is an example of how, as in prism/grating pairs, chirped mirror pairs can

also be used in combination with other dispersion pre-compensation methods.

2.2.3 Pulse shapers

Pulse shapers are extremely flexible tools that are capable of arbitrarily modifying all orders of dispersion in an ultrashort laser pulse[38]. Although pulse shapers themselves do not measure dispersion, they can compensate for all orders of dispersion in a microscope system, once this dispersion has been measured. Pulse shapers can also be used to implement an algorithm that does measure dispersion, as will be discussed later.

Pulse shapers come in many varieties, including those based on acoustic-optical modulators, fixed spatial masks, and liquid-crystal spatial light modulators (SLMs). Although fixed spatial masks are inexpensive, acoustic-optical modulators and SLMs have the advantage of being easily reconfigurable via computer control. Both acoustic-optic modulators and SLMs are popular for ultrashort pulse shaping; however, this discussion will focus on pulse shapers based on liquid crystal SLMs, the variety that is used for the experiments in this work.

Figure 2.5 shows the basic layout of a Fourier transform pulse shaper. The pulse shaper uses gratings (or sometimes prisms) to expand the beam into its constituent frequencies. A cylindrical lens focuses the spread spectrum into a thin line that covers all the pixels in 1-D liquid-crystal SLM. A computer controls the SLM, instructing it to apply different voltages to the various pixels. Each pixel contains birefringent liquid crystal which rotates depending on the amount of voltage applied, adding different amounts of phase delay to the narrow frequency ranges covered by each pixel. With the addition of a second layer of pixels and a polariser, the amplitude of these frequencies can be changed as well. On the other side of the SLM, a second lens and grating collects the spread spectrum and recombines it into a single collinear spot. Many variations of this basic geometry exist; some designs use prisms instead of gratings (for higher efficiency), or focus using cylindrical mirrors instead of lenses (to reduce

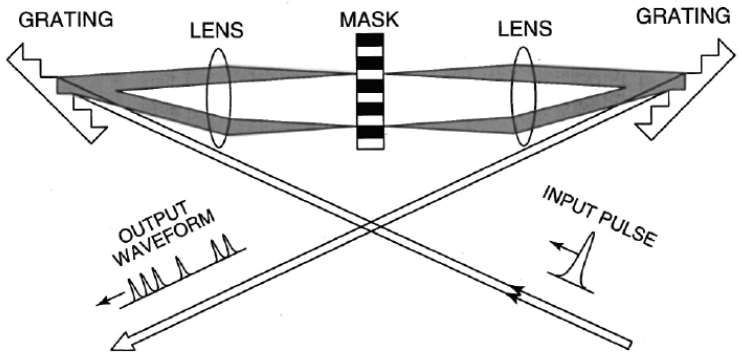

Figure 2.5:
Basic configuration of the Fourier transform pulse shaper. The input pulse is spread into its spectral components by the grating and focused using a cylindrical lens onto a 1-D liquid crystal spatial light modulator (or fixed phase mask, as shown here). The spatial light modulator applies a computer-controlled amount of phase delay (dispersion) to each wavelength, and another lens/grating combination recombines the wavelengths into a spatially-uniform pulse. Image is from [38].

dispersion within the shaper), or insert a mirror after the SLM, doubling the amount of phase delay the SLM can impart and halving the amount of optics in the system.

Although pulse shapers are extremely flexible ways of controlling dispersion, they do suffer from some hardware-imposed limitations. Due to the placement of gratings (and the presence of prisms and lenses, if used), shapers introduce some amount of dispersion into the system. However, by adjusting the grating/prism placement, the amount of dispersion can be minimised or even made into negative 2nd order dispersion, cancelling some of the positive 2nd order dispersion of microscope systems. Shapers also introduce small amounts of spatial chirp (uneven frequency distribution across the beam profile) that can change slightly as different phase functions are applied to the pulse[39].

SLM pulse shapers also can produce only a limited amount of dispersion compensation, due to their discrete number of pixels, and the limited amount of phase delay produced by each SLM pixel. In a typical SLM, each pixel may be able to produce a phase delay between 0 and 2π, so to produce a 2.1π phase delay

at a particular pixel, the SLM applies the equivalent delay of 0.1π. This can become a problem when the neighbouring pixel has a value of, say, 2π – there is now a sharp jump from 2π to 0.1π between the pixels (this is called wrapping). These sharp jumps between pixels are smoothed out due to pixel cross-talk (leakage between neighbouring pixels). Therefore, a wrap from 2π to 0.1π will not go sharply between these two values. The effect is not noticeable on isolated wrapping, but causes phase inaccuracies as well as amplitude modulation when the SLM is trying to apply a phase function with a closely-spaced series of wraps[39]. And unfortunately, applying large amounts of negative 2nd order dispersion, such as that needed to cancel the dispersion in a microscope system, requires the SLM to implement a quadratic phase function with very steeply sloped edges, producing large amounts of wrapping.

There are several approaches that can be used to mitigate the problem of excessive wrapping. A simple solution is to use an SLM with more pixels, increasing the number of pixels between wraps – unfortunately this can significantly increase the cost of the SLM. Another approach is to reduce the amount of 2nd order dispersion that the SLM has to compensate. This can be done by introducing negative 2nd order dispersion by adjusting the grating position (as mentioned above), and/or by using the shaper in combination with prism/grating precompressor or chirped mirrors.

2.3 Dispersion measurement

The use of prism/grating precompressors, the design of chirped mirrors, and in particular the use of pulse shapers, is dependent on knowing the amount of dispersion present in the system, at least to some degree. The more accurately dispersion is known, the easier it is to place prisms/gratings at the right distance in precompressors, to design chirped mirrors that more completely compensate the system's dispersion, or to choose the correct compensating phase function to be implemented by the pulse shaper. When using dispersion compensation

methods that compensate for most, but not all, dispersion, it is important to know the final pulse duration at the sample, for comparison with theory or with similar experiments performed on other systems. For most of these applications, it is important to measure higher orders of dispersion as well as 2nd order dispersion. In other words, the goal is to learn the phase function that the entire optical system imparts on the pulses.

Although dispersion can be calculated from the wavelength-dependent refractive indexes of the materials the beam passes through, and its path length in each material, these calculations become frightfully complex in microscope systems. Path lengths in particular are hard to accurately estimate, and the composition of dielectric mirrors or anti-reflection coatings (especially those in microscope objectives) may be proprietary. In complex microscope systems, the best choice is to experimentally determine dispersion. Numerous methods have been proposed and demonstrated for measuring dispersion in microscope systems. I will briefly review one commercially-available method of dispersion measurement, followed in Section 2.4 by two methods for combined dispersion measurement and compensation.

2.3.1 Frequency Resolved Optical Gating (FROG)

Frequency-Resolved Optical Gating (FROG) is a popular method for measuring dispersion in ultrashort pulses[40]. Numerous variations of the basic algorithm and hardware exist; collinear SHG-FROG is the version specially adapted for use in microscope systems.

The algorithm is centred around the idea of autocorrelation: using a short pulse to measure itself. In traditional autocorrelation, a pulse is split in an interferometer, with adjustable delay introduced to one of the interferometer arms. The pulses in each arm of the interferometer are overlapped in some nonlinear media, such as a second harmonic generating crystal, which generates a signal that, when integrated over time by a detector, produces a second-order autocorrelation of the original signal (Figure 2.6).

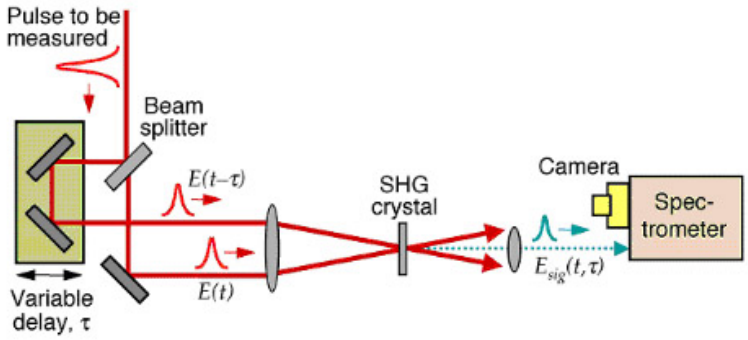

Figure 2.6:
Basic autocorrelation setup used to measure ultrashort pulses. Image credit: Swamp Optics.

Traditional autocorrelation provides a rough measure of the length of a pulse, but not an accurate depiction of the pulse's structure in time. It cannot be used to calculate the pulse's spectral phase function (the amount of dispersion it has undergone).

FROG measurements utilise a form of autocorrelation that includes frequency information as well, by interfering the pulse with a frequency-limited version of itself. Scanning the window of limited frequencies produces a picture of the pulse in time and frequency, called a spectrogram. The spectrogram contains enough information to recover the pulse's spectral phase (except for a direction vs time ambiguity which can be resolved with extra information). This recovery is done via closed-loop algorithms (such as genetic algorithms).

The original SHG-FROG hardware requires the pulse to be split via a beamsplitter and recombined at a second harmonic generation (SHG) crystal. However, in microscope systems, sending two beams to the sample along two different optical paths introduces problems with back aperture filling, and slight differences in the amount of dispersion each beam encounters[41]. A number of research teams have developed versions of SHG-FROG that are collinear, allowing them to be used to measure pulse duration at a microscope sample[41, 42, 43].

It should be noted that FROG is meant for pulse characterisation only – the method itself does not compensate for the dispersion it finds. When researchers

use FROG as part of a dispersion compensation strategy, they need to use dispersion compensation methods (such as those outlined above) to compensate for the dispersion they have measured[44]. Although FROG has been used in combination with pulse shapers to compensate dispersion in optical fibre systems[44], there are no reports so far of ultrashort (<50fs) pulses compressed to TL at the microscope sample plane using information from FROG.

2.4 Dispersion measurement and compensation

2.4.1 Multiphoton Intrapulse Interference Phase Scan (MIIPS)

Multiphoton Intrapulse Interference Phase Scan (MIIPS) is the method used in this thesis for simultaneously measuring and compensating dispersion. Recently introduced by researchers at Michigan State University[45, 24, 46], MIIPS is single-beam and non-interferometric and therefore adapts well to use in microscope systems[24]. In this thesis we demonstrate its first use in an optical trapping system. We also show the first use of the MIIPS method to produce dispersion-compensated ultrashort Bessel beams.

MIIPS requires two primary components: a pulse shaper to be placed somewhere in the beam path, and a second harmonic generation (SHG) medium (such as KDP or BBO) at the sample plane where dispersion is to be measured and compensated (see block diagram in Figure 2.7). MIIPS measures spectral phase based on the change in the SHG spectrum as the pulse shaper applies known phase functions to the beam's spectral profile. Below, we describe the MIIPS algorithm in more detail.

The unknown dispersion that an optical system applies to the laser pulses can be expressed as a spectral phase function $\Phi(\omega)$. Note that $\Phi(\omega)$ is not merely quadratic, but may have a complex form.

The pulse shaper adds a known phase function $f(\omega)$ to the unknown phase

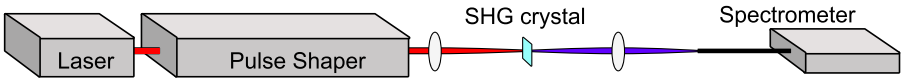

Figure 2.7:
Block diagram of the Multiphoton Intrapulse Interference Phase Scan (MIIPS) method for dispersion measurement and compensation. At the heart of the MIIPS method is a pulse shaper, which can be placed at any point between the laser and the sample plane where dispersion is to be measured and compensated. A second harmonic generation (SHG) medium such as a BBO crystal must be placed at the sample plane. MIIPS will measure the total dispersion of the system from the laser to the SHG crystal. In this block diagram, a lens is used to focus the laser onto the SHG crystal - in practise, the optical path can include anything from a lens to an optical fibre to an entire microscope system. A spectrometer (fibre spectrometer shown here) collects the SHG signal. Figure is based on [46].

function, producing a total phase function at the sample plane,

$$\phi(\omega) = \Phi(\omega) + f(\omega) \tag{2.5}$$

If a SHG-active material (such as a BBO crystal) is placed at the sample plane, the resulting SHG signal will be proportional to

$$I^{(2)}(2\omega) = \left|\mathcal{E}^{(2)}(2\omega)\right|^2 \tag{2.6}$$

where $\mathcal{E}^{(2)}(2\omega)$ is the frequency-doubled electric field produced by second harmonic generation. $\mathcal{E}^{(2)}(2\omega)$ can be thought of as the effective second-harmonic field available for two-photon excitation. For two-photon fluorescence, for example, the actual two-photon absorption at a frequency 2ω can be determined by multiplying $\mathcal{E}^{(2)}(2\omega)$ by the molecule's two-photon absorption cross section.

To obtain an expression for $\mathcal{E}^{(2)}(2\omega)$, note that the electric field of the laser pulse at the sample plane is

$$\mathcal{E}(t) = E(t)e^{i\phi(t)} \tag{2.7}$$

or in frequency domain form,

$$\mathcal{E}(\omega) = E(\omega)e^{i\phi(\omega)} \tag{2.8}$$

In the time domain, the frequency-doubled electric field is the square of the fundamental field:

$$\mathcal{E}^{(2)}(t) = \mathcal{E}(t)\mathcal{E}(t) \tag{2.9}$$

which in the frequency domain can be expressed as the convolution of $\mathcal{E}(\omega)$ with itself.

$$\mathcal{E}^{(2)}(\omega) = \int \mathcal{E}(\omega')\mathcal{E}(\omega - \omega')d\omega' \tag{2.10}$$

By changing variables, the convolution integral can be written in the form

$$\begin{aligned} \mathcal{E}^{(2)}(2\omega) &= \int \mathcal{E}(\omega + \Omega)\mathcal{E}(\omega - \Omega)d\Omega \\ &= \int E(\omega + \Omega)E(\omega - \Omega)e^{i[\phi(\omega+\Omega)+\phi(\omega-\Omega)]}d\Omega \end{aligned} \tag{2.11}$$

Here, ω' and Ω are dummy integration variables. Then,

$$I^{(2)}(2\omega) = \left| \int E(\omega + \Omega)E(\omega - \Omega)e^{i[\phi(\omega+\Omega)+\phi(\omega-\Omega)]} \right|^2 \tag{2.12}$$

Equation 2.12 indicates that the SHG signal at frequency 2ω is produced by the interference between all possible combinations of frequency pairs in the pulse symmetrically spaced around ω, a concept called multiphoton intrapulse interference[47].

$I^{(2)}(2\omega)$ is maximum when the exponent in Equation 2.12 is equal to 1; that is, when $\phi(\omega + \Omega) + \phi(\omega - \Omega) = 0$. Therefore, the observed SHG spectrum will have a maximum at frequency 2ω if all of the frequency pairs symmetric about ω have ϕ that add constructively. Pulses with zero net dispersion at the crystal plane, also known as transform-limited (TL) pulses, have $\phi(\omega) = 0$ and therefore have the maximum possible SHG intensity at every frequency. Observing the

locations of peaks in the SHG spectrum gives us information about the phase function's degree of symmetry about each frequency.

Even more importantly, the locations of the SHG peaks allow one to obtain a direct measurement of the phase function's second derivative, $\phi"(\omega)$. By integrating $\phi"(\omega)$ we can obtain full knowledge of the pulse's phase function (and therefore temporal profile), except for the zeroth order and 1st derivative phases. However, these two terms, as given in the Taylor expansion of $\phi(\omega)$ below, do not significantly affect the pulse profile.

$$\phi(\omega) = \phi(\omega_0) + \phi'(\omega_0)(\omega - \omega_0) + \frac{1}{2}\phi"(\omega_0)(\omega - \omega_0)^2 + \frac{1}{3}\phi^{(3)}(\omega_0)(\omega - \omega_0)^3 + ... \tag{2.13}$$

The zeroth order term $\phi(\omega_0)$ is the absolute phase, which determines the position of individual carrier frequency oscillations within the pulse's temporal envelope. For pulses more than a few optical cycles long, $\phi(\omega_0)$ has little effect on the pulse envelope, or on interaction with materials. The first derivative term $\phi'(\omega_0)$ is the first order phase, which determines the absolute arrival of the pulse in time. All frequencies are equally delayed by $\phi'(\omega)$, however, so this term does not affect the temporal profile or nonlinear excitation. Therefore, we only need to find $\phi"(\omega)$ to determine the pulse spectral phase function (and therefore to be able to use the built-in MIIPS pulse shaper to compensate for the spectral phase introduced by our optical system).

To understand how the MIIPS algorithm measures $\phi"(\omega)$, examine the Taylor expansion of $\phi(\omega + \Omega) + \phi(\omega - \Omega)$:

$$\phi(\omega + \Omega) + \phi(\omega - \Omega) = 2\phi(\omega) + \phi"(\omega)\Omega^2 + \ldots + \frac{2}{(2n)!}\phi^{(2n)}(\omega)\Omega^{2n} \tag{2.14}$$

which is minimum for all Ω when $\phi"(\omega) = 0$. Here, we ignore the effects of higher-order terms, to first approximation. Remember that $\phi(\omega)$ is the sum of our unknown dispersion function $\Phi(\omega)$ and a known $f(\omega)$ introduced by the pulse shaper. Since $\phi"(\omega) = \Phi"(\omega) + f"(\omega)$, when $\phi"(\omega_0) = 0$ for some frequency

ω_0 (corresponding to a SHG peak at $2\omega_0$), $f(\omega_0)$ has locally compensated the dispersion $\Phi(\omega_0)$. We therefore have $\Phi"(\omega_0) = -f"(\omega_0)$, which is known, so we have sampled $\Phi"(\omega)$ at every frequency ω_0 corresponding to maxima in the SHG spectrum $I^{(2)}(2\omega)$ at $2\omega_0$. To sample $\Phi"(\omega)$ at all the other ω in the pulse profile, we only need to use a number of different $f(\omega, p)$, usually by choosing a function type and a parameter p to scan.

One of the simplest $f(\omega, p)$ is $f_1(\omega, p) = -p(\omega - \omega_c)^2$, a quadratic phase function where p is the scanning parameter and ω_c is a constant frequency at which the phase function is chosen to be centred. $f_1"(\omega, p)$ is simply a straight line. Figure 2.8 a) shows a set of these $f_1"(\omega, p)$ plotted as horizontal dotted lines. An example unknown $\Phi"(\omega)$ is shown as a solid blue line. A red dot marks the intersection points of $-f_1"(\omega, p)$ and $\Phi"(\omega)$, where these two functions cancel each other and the net phase $\phi"(\omega) = 0$. Figure 2.8 b) sketches the SHG spectra $I^{(2)}(2\omega)$ that would be measured using each $f_1(\omega, p)$. Note that each SHG maximum corresponds to an intersection point of $f_1"(\omega, p)$ and $\Phi"(\omega)$. Using a finely spaced set of $f_1"(\omega, p)$ allows $\Phi"(\omega)$ to be measured to high precision.

The most commonly used $f(\omega, p)$ is a sinusoidal phase function, $f(\omega) = -\alpha\gamma^2 sin\,[\gamma(\omega - \omega_0) - p]$, which samples $\Phi"(\omega)$ as shown in Figure 2.9.

As described above, scanning $f(\omega, p)$ directly measures $\Phi"(\omega)$. To cancel phase distortion, the pulse shaper can add the inverse phase, $-\Phi(\omega)$ to get a net phase function of zero. (Again, Φ_0 and Φ' are ignored, since they do not affect multiphoton processes for our pulses.) In practise, the MIIPS algorithm is usually repeated at this point to refine the measurement of $\Phi"(\omega)$. In addition to exactly cancelling the measured dispersion to obtain transform-limited pulses at the sample plane, the pulse shaper can be used to add arbitrary phase functions to the compensation function, creating custom-tailored pulses at the sample plane. A variant of the MIIPS algorithm exists that does not require a pulse shaper, but offers dispersion measurement only, and does not compensate for the dispersion it finds[48].

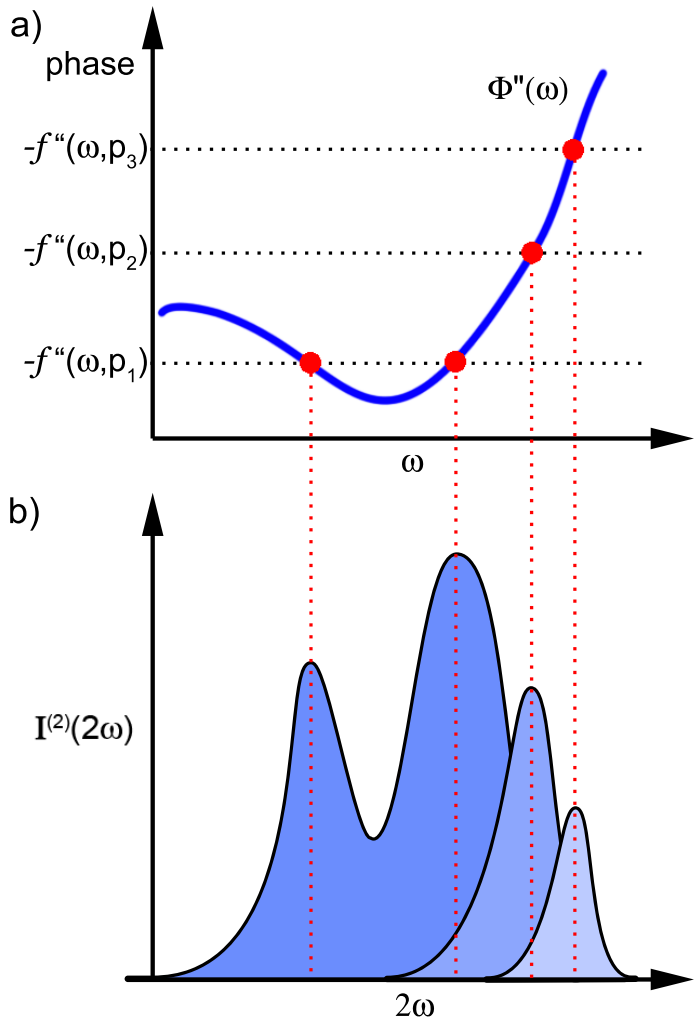

Figure 2.8:
Cartoon showing how MIIPS measures the second derivative of an unknown phase function $\Phi"(\omega)$. a) Parametrised test functions $-f"(\omega, p)$ plotted as dotted horizontal lines against a sample $\Phi"(\omega)$. Intersection points (shown as red dots) are where the $-f"(\omega, p)$ exactly cancel $\Phi"(\omega)$, so $\Phi"(\omega) = f"(\omega, p)$ at these intersection points. b) Sketch of the SHG peaks that correspond to each intersection point of $\Phi"(\omega)$ and $f"(\omega, p)$. Each value of the scanning parameter p allows $\Phi"(\omega)$ to be sampled at a different point or points. The amplitude of each peak is determined by the pulse's spectral profile $E(\omega)$. Figure is based on [48].

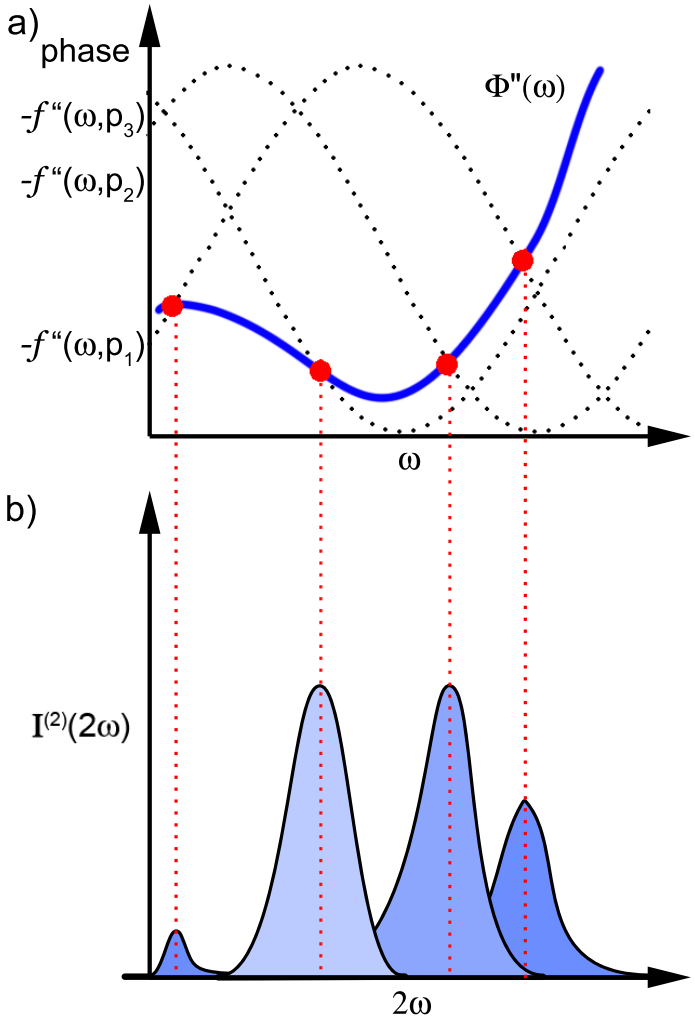

Figure 2.9:
Cartoon illustrating the MIIPS measurement of an unknown phase function $\Phi"(\omega)$. a) The same unknown $\Phi"(\omega)$ as in Figure 2.8, but shown with sinusoidal $-f"(\omega, p)$ rather than quadratic. These sinusoidal functions sample $\Phi"(\omega)$ at each point where they intersect. b) Sketch of the SHG signal resulting from the different $-f"(\omega, p)$ as p is scanned. As in Figure 2.8, the SHG peaks correspond to frequencies where the unknown $\Phi"(\omega)$ equal the known $f"(\omega, p)$.

2.4.2 Spectral Shear Interferometry for Direct Electric Field Reconstruction (SPIDER)

Recently-introduced variants of Spectral Shear Interferometry for Direct Electric Field Reconstruction (SPIDER) have the ability to both measure and compensate for dispersion in microscope systems[49, 50]. Like MIIPS, these versions of SPIDER use a pulse shaper as part of the phase measurement algorithm, and can therefore use this same pulse shaper to add the inverse of the measured dispersion, cancelling out dispersion at the sample. Although earlier versions of SPIDER are commercially available, these new versions are still in development.

2.5 Conclusion

In the discussion above, we have outlined the reasons that temporal dispersion occurs when sending ultrashort laser pulses through high-NA microscope systems, as well as a few approaches for managing dispersion. Some strategies such as prism/grating precompressors and chirped mirror pairs offer relatively inexpensive and simple compensation of large amounts of 2nd order dispersion. Prism/grating precompressors offer a continuous and wide range of 2nd order dispersion compensation levels, but introduce higher order dispersion, preventing them from compressing pulses below about 30fs FWHM pulse duration. Chirped mirror pairs can provide custom amounts of 2nd order and higher order dispersion compensation, but these amounts are fixed and cannot be finely adjusted for inserting or replacing filters, microscope objectives, etc. Liquid crystal SLM pulse shapers, although more complex, can produce arbitrary 2nd order and higher order phase functions with switching rates of tens of milliseconds. These methods have been used to compress pulses, both alone and in combination with other methods. Without an accurate measure of dispersion at the sample, however, the dispersion compensation will be noticeably incomplete for ultrashort pulses.

A number of strategies exist for measuring dispersion, although only some

of them can be used in the restricted geometry of microscope systems. Additionally, only a few methods allow the measurement of higher-order dispersion. Collinear SHG-FROG is one such method, although it only measures and does not compensate dispersion by itself. FROG has been used in combination with pulse shapers to compensate dispersion in optical fibre systems, but so far has not been used to compress ultrashort (<50fs) pulses in microscope systems.

MIIPS is a recently-introduced method that uses a pulse shaper to measure and compensate 2nd order and higher-order phase distortions in a variety of optical systems, including microscopes. MIIPS incorporates a pulse shaper, so a system with MIIPS also has the capability of applying arbitrary phase functions to the dispersion compensation function, producing a reproducible custom-tailored pulse at the sample plane. MIIPS is commercially available for use in microscope systems; this thesis represents the first description of its use in an optical trapping system or for studies of ultrashort Bessel beams.

Another method that offers dispersion measurement and compensation in ultrashort pulses is SPIDER. Although earlier versions of SPIDER used multiple interfering beams, recently-introduced variants of SPIDER are collinear and can be used in microscope systems. Like MIIPS, these versions of SPIDER incorporate a pulse shaper which can therefore be used to compensate for measured dispersion, and to apply custom pulse shapes. Although earlier versions of SPIDER are commercially available, these newer collinear versions are still in development.

The next chapter describes the use of the MIIPS method for simultaneous dispersion measurement and compensation in an optical trapping system, while Chapter 5 describes MIIPS dispersion measurement and compensation in a Bessel beam photoporation system.

Chapter 3

Development of the experimental setup

3.1 Laser system

The experiments presented here were carried out using a titanium sapphire oscillator (Femtolasers FemtoSource) capable of producing 12fs full width at half maximum (FWHM) pulses centred at 800nm, at a repetition rate of 80MHz. The laser's spectral shape varied depending on cavity alignment, but typically had a 90nm FWHM bandwidth (see Figure 3.1). The laser's output power was a maximum of 1W continuous-wave, and 800mW mode-locked; typical values were 500-600mW mode-locked.

Since part of the laser cavity is external to the manufacturer-provided enclosure, we needed to use an additional custom-built enclosure to protect the laser from dust, air currents, and temperature fluctuations. This enclosure was slightly modified from an earlier design by a co-worker Jill Morris, to accommodate a change in the orientation of the laser cavity.

The output power, spectral shape, and stability were very sensitive to cavity alignment. Cavity alignment tended to shift overnight, so power and stability

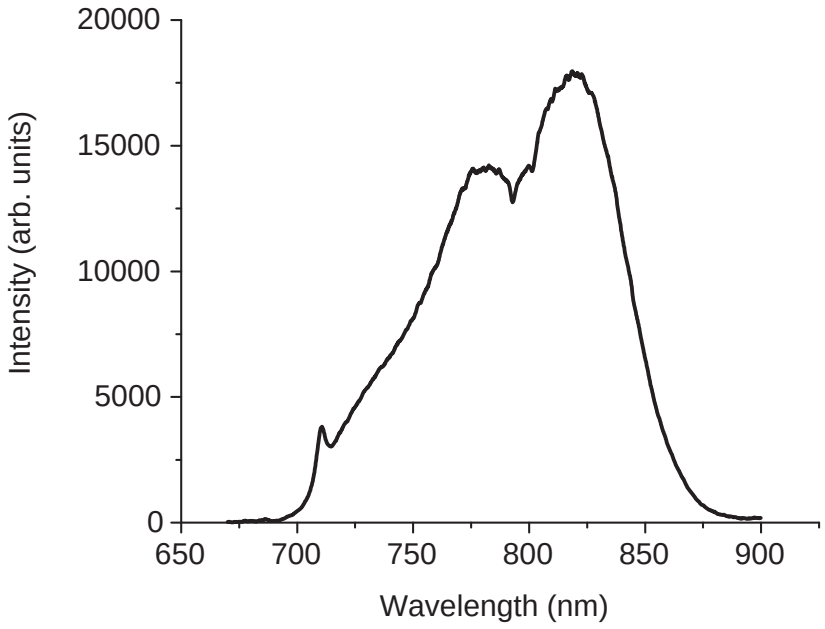

Figure 3.1:
Laser's typical fundamental spectrum, measured with a USB 4000 fibre spectrometer through a non-absorbing scatterer (lens tissue).

had to be re-optimised on most days. We treated stability as the most important parameter to be optimised, which was usually, but not always, correlated with maximum power. When cavity alignment shifted, the cavity dispersion would usually shift as well. We determined that the output coupler mount was responsible for much of the shifting; this was the part that would most often have to be adjusted to correct the power and stability loss, and the actuator screws were not moving smoothly. Removing the output coupler and cleaning the threads on the mount's thumbscrews did improve the stability temporarily. Cavity shifts could not be completely avoided, so we had to periodically check the laser's dispersion (using MIIPS, as described below) and output power, adjusting the cavity alignment and remeasuring dispersion as necessary.

3.2 System overview

The experiments in this thesis used a number of homemade microscopes. Initial experiments carried out before the arrival of the MIIPS pulse shaper verified that optical trapping was possible using the laser in mode-locked mode. Upon the arrival of the MIIPS system, we took the opportunity to shift experiments to a basement laboratory with floatable optical table, where vibrations would be diminished. Having an empty table and bare shelves to start with gave us the freedom to design a setup that included the pulse shaper, an optical trapping microscope with a spectrometer that detected back-scattered signal from the sample plane, and an axicon system. A photograph of the full system is shown in Figure 3.2, a block diagram is shown in Figure 3.3, and the individual components are described below.

Upon exit from the laser, the beam height is adjusted via a periscope, and the beam diameter is expanded by a factor of two to 6 mm. The beam then enters a pulse shaper, custom-built by BioPhotonic Solutions, Inc. The shaper includes a grating to spread the beam into its constituent frequencies, and a computer-controlled 640-pixel liquid crystal spatial light modulator (SLM) to modify the phase and/or amplitude of each of the beam's frequencies. The frequencies are recollected and recollimated via grating before leaving the shaper. Approximately 30% of the power that enters the shaper is transmitted, with most of the power loss due to higher-order diffraction from the gratings. For details about this kind of shaper, see Section 2.2.3. Section 3.4 below describes the alignment, testing, and use of this shaper for dispersion compensation.

Shortly after the beam exits the pulse shaper, a flip mirror selects between the optical trapping system and the axicon system. A block diagram showing the major components of the optical system is shown in Figure 3.3. The optical trapping system is described in the following sections, and the axicon system is described in Chapter 5.

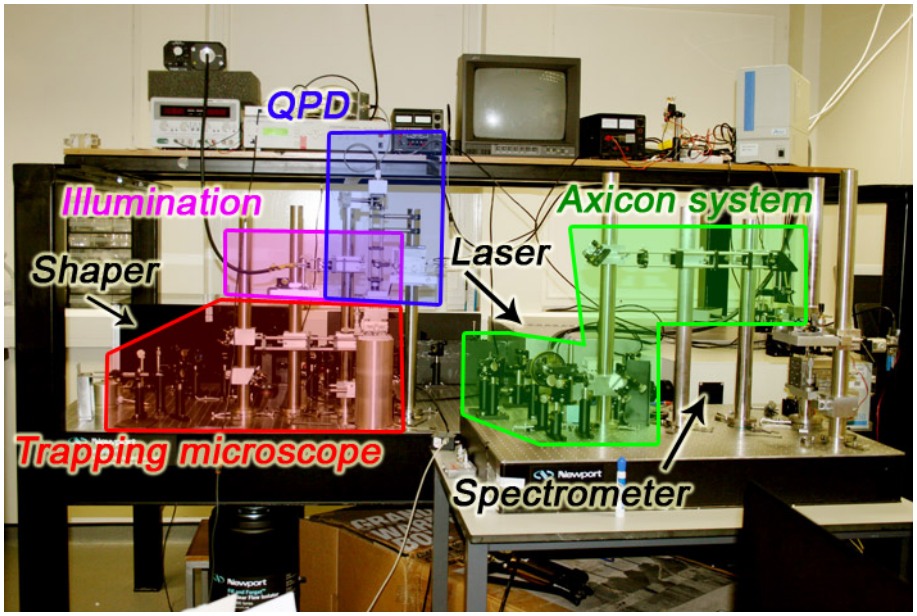

Figure 3.2:
Photograph of entire setup for the experiments described in this thesis (also see block diagram in Figure 3.3). The ultrashort laser source is a 12fs Ti:Sapphire 80MHz pulsed system from FemtoLasers (FemtoSource Scientific Pro), protected from dust and airflow by a custom-built enclosure, visible as a grey metallic box in the back right. The pulse shaper (black enclosure) is visible at back left. At front left (outlined in red) is the trapping microscope. Its illumination (outlined in magenta) and quadrant photodiode (QPD) position detection (outlined in blue, and shown in more detail in Figure 3.5) systems can be replaced with a second harmonic collection system for dispersion measurement (not shown). For a more detailed view of the trapping microscope, see Figure 3.4. At middle right is a Jobin-Yvon Triax 550 monochromator, coupled to a Jobin-Yvon Symphony Solo CCD camera (beige enclosure). The axicon system (outlined in green) is located on an auxiliary (non-floated) table at the front right; vibrations are less critical in this setup, and a pair of irises allows the slow drift in the floated table height to be corrected. For a more detailed photo, diagram, and description of the axicon setup, see Figures 5.1 and 5.2 in Section 5.2. Computers to the left of the optical table control the pulse shaper, USB 4000 spectrometer, QPD position detection, and image acquisition. Another computer (monitor just visible at far right) controls the monochromator/CCD spectrometer system.

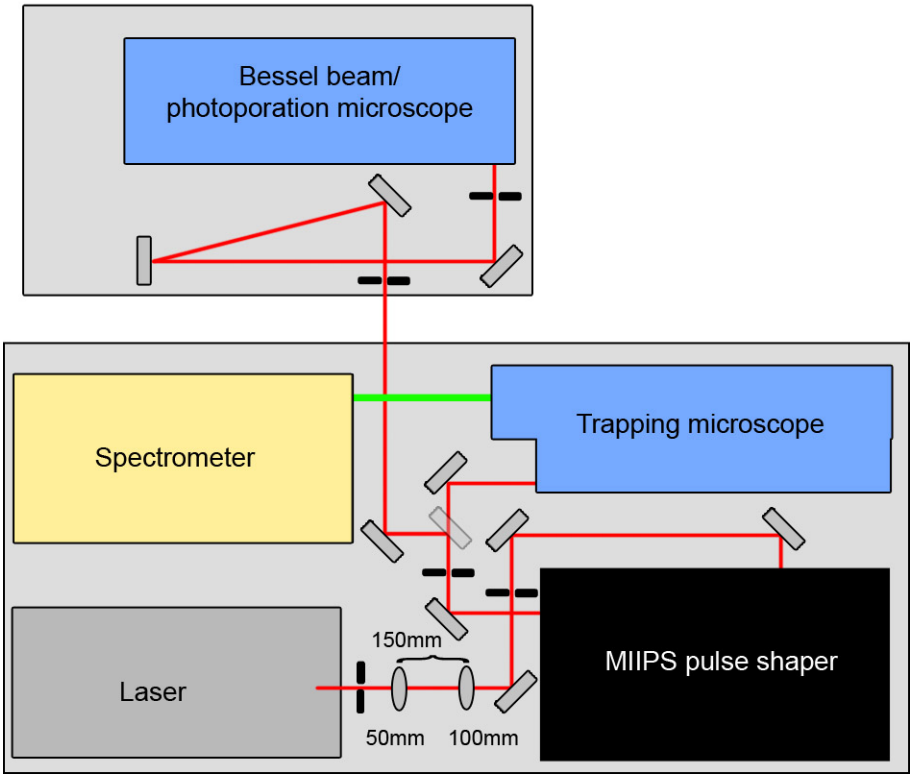

Figure 3.3:
Block diagram depicting the full system used in this thesis. The laser is a 12fs, 80MHz Ti:Sapphire laser from FemtoLasers, which produces CW or mode-locked pulses centred at 800nm. The MIIPS pulse shaper was custom-built by BioPhotonic Solutions, Inc., and contains a 640-pixel spatial light modulator from CRi. After the beam exits the shaper, a flip mirror (shown translucent) selects between the trapping microscope and the axicon system (both home-built). The path length into the axicon system is extended to allow a long distance between two important alignment irises, which allow alignment to be corrected for the relative drift between the two optical tables. The trapping microscope includes a spectrometer consisting of a Jobin-Yvon Triax 550 monochromator, coupled to a Jobin-Yvon Symphony Solo CCD camera.

3.2.1 Trapping microscope

A diagram of the trapping microscope is shown in Figure 3.4. After the shaper, the beam diameter is expanded by a factor of 2 to overfill the back aperture of the objective used[51], and sent to a periscope at the entrance of a home-built microscope. A set of 100mm lenses forms a 1:1 telescope that can be used together with the periscope mirrors to steer the beam in xy. In practise the beam's position in the sample was steered both lateral to the beam propagation (in x, y) and axially (in z) by translating the sample stage itself using an xyz stage; this is to allow steering in the z direction, avoid misalignment, and avoid possible differences in dispersion within the objective as the beam is steered. The sample stage is mounted on a custom-machined block of solid metal, to reduce sample stage vibrations.

A quarter wave plate is used to circularly polarise the beam, since it was found that a linearly polarised beam would create a trap with different stiffnesses in the x and y directions. Although we incorporated and dispersion-compensated a variety of microscope objectives, the trapping work described here is performed with a 100x 1.40NA Nikon Plan Apo DIC H oil immersion objective. The sample is illuminated from above via a 40x 0.65NA Nikon 40x E Plan objective; this same objective collects transmitted laser light from the sample plane and sends it to a quadrant photodiode (QPD) for position detection, as described below in Section 3.3. A dichroic mirror sends the laser up to the sample plane and passes white-light illumination from the OSL1-EC fibre light source (as well as a small portion of back-reflected laser light) through a 200mm tube lens, which images the focal plane onto a CCD camera.

Below the dichroic mirror is a 50/50 beamsplitter that picks off half of the illumination/fluorescence and sends it to a spectrometer consisting of a Jobin-Yvon Triax 550 monochromator, coupled to a Jobin-Yvon Symphony Solo CCD camera. An demagnifying telescope consisting of a 200mm and a 100mm lens decreases the diameter of the signal beam by a factor of 2, and a short-pass filter (Comar GK 575) removes any remaining back-reflected laser signal. A 50mm

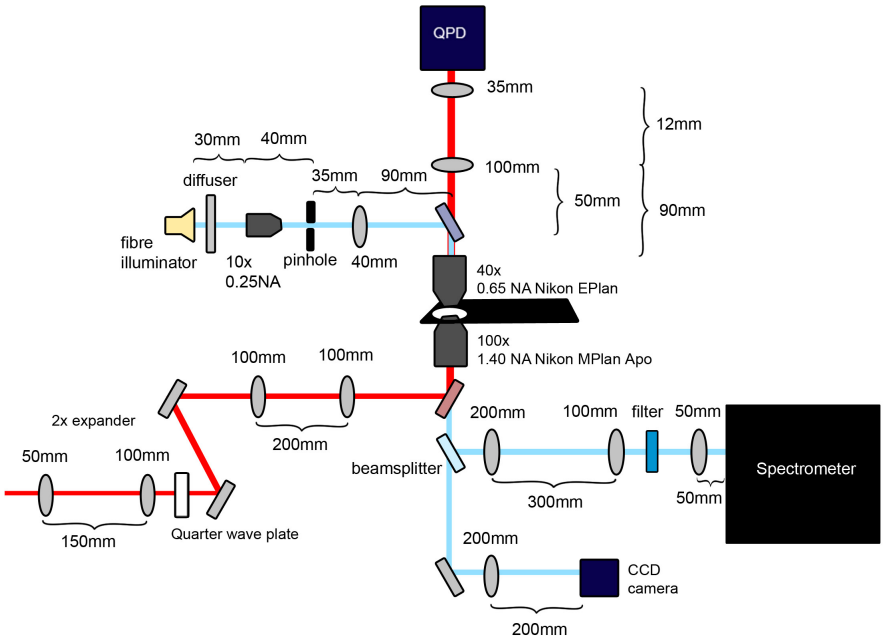

Figure 3.4:
Custom-built trapping microscope, with quadrant photodiode (QPD) position detection, white light illumination, CCD imaging, and spectrometer detection of signal in the sample plane. The beam enters at the lower left of the figure, from the output of the pulse shaper.

lens focuses the signal onto the entrance slit of the spectrometer.

3.3 Position detection

As part of our investigations, we needed to be able to determine the trap stiffness under a number of different experimental parameters. The motion of a trapped particle in viscous medium can be described by an over-damped harmonic oscillator. The trapped particle experiences a restoring force toward the centre of the optical trap, which is the product of the trap stiffness and the trapped particle's displacement from the trap centre. The trap stiffness can therefore be determined by observing the particle's motion in the trap, using the particle's position distribution or an analysis of the frequency of the particle's motion. Both methods require accurate detection of the particle's position within the

optical trap.

We used back focal plane interferometry-based position sensing[52] to detect the position of the particle within the laser focus. (See Figure 3.4 for a diagram and Figure 3.5 for a photograph.) Transmitted laser light from the sample plane is collected through a 0.65NA 40x Nikon E Plan objective, and loosely focused onto a quadrant photodiode (QPD) using a series of two lenses. The individual signals from each quadrant are amplified separately with a home-built analog amplifier, and converted to digital form using a National Instruments USB-9162 data acquisition card. This yields four individual time traces, one from each quadrant, which can be converted to x, y, and z position using the equations

$$x = \frac{(A-B)+(C-D)}{(A+B+C+D)} \tag{3.1}$$

$$y = \frac{(A-C)+(B-D)}{(A+B+C+D)} \tag{3.2}$$

$$z = A+B+C+D \tag{3.3}$$

These data acquisitions and calculations were performed using an adaptation of a LabView program originally written by Peter Reece.

A check that the scattered light signal is centred on to the QPD is to ensure that the four quadrant traces have the same average value, and that the sum of the four averages is maximised. Another check is to plot a histogram of the measured x, y, and z positions over a period of time; with a long enough acquisition time, the histograms should have a Gaussian shape. Any other shape indicates a possible alignment issue.

The stiffness of the trap can be calculated from the width of the x, y, or z position histogram (a wider histogram means more fluctuation in particle position and thus a weaker trap), or from the power spectrum of the x, y, or z time trace. By fitting a Lorentzian curve to the power spectrum, the rolloff frequency of the Lorentzian function can be obtained. This rolloff frequency can be directly converted to trap stiffness using the equation

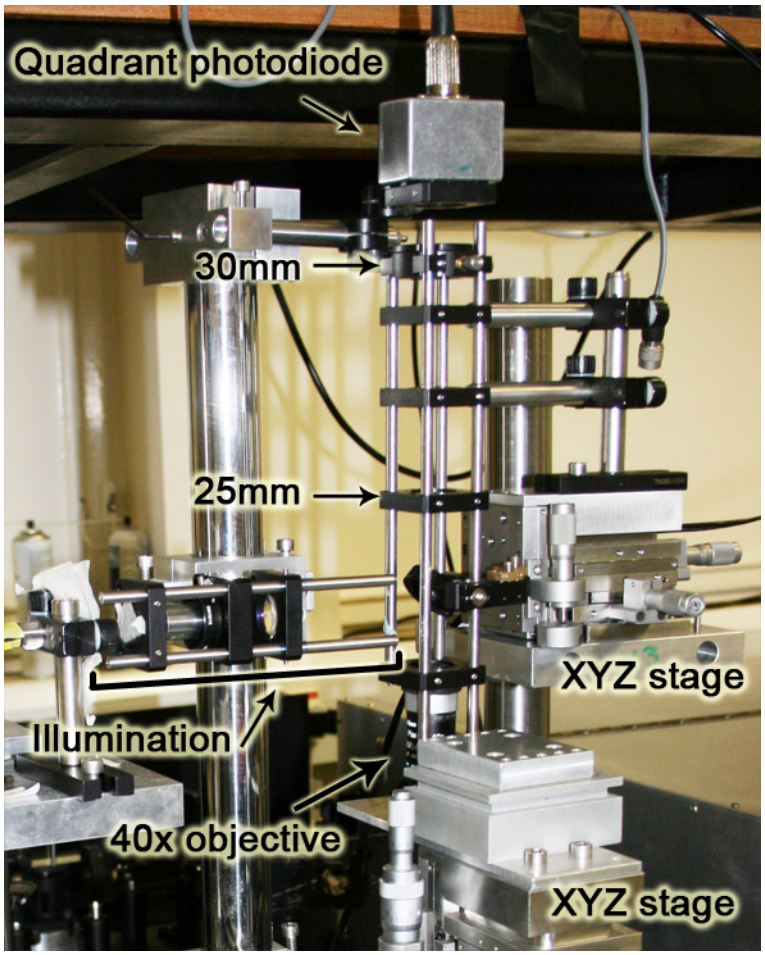

Figure 3.5:
Photograph of quadrant photodiode (QPD) back focal-plane interferometry position detection. A 40x Nikon E Plan 0.65NA objective collects transmitted light from the sample plane, which passes through a dichroic mirror (used for coupling in illumination), and a combination of a 100mm lens and a 35mm lens which loosely focus the resulting diffraction pattern onto the QPD. The four QPD signals pass through a home-built amplifier and are sent to the computer for processing via National Instruments USB 9162 data acquisition card.

$$k = 2\pi\gamma f_c \tag{3.4}$$

where k is the trap stiffness, f_c is the cutoff frequency, and γ is the drag coefficient, given by

$$\gamma = \frac{6\pi\eta r p}{\left(1 - \frac{9}{16}\frac{r}{h} + \frac{1}{8}\left(\frac{r}{h}\right)^3 - \frac{45}{256}\left(\frac{r}{h}\right)^4 - \frac{1}{16}\left(\frac{r}{h}\right)^5\right)} \tag{3.5}$$

Here, r is the particle radius, h is the distance from the glass surface, η is the viscosity of the medium, and p is the density of the particle[53].

3.4 Dispersion measurement and compensation

3.4.1 Setup

As mentioned above, we use the MIIPS method for measuring and compensating the dispersion of our system[45, 24, 46]. This method makes use of a pulse shaper[38]; the pulse shaper we used was sent to us from BioPhotonic Solutions, Inc of Okemos, Michigan, USA, as part of a collaboration that I initiated with my previous research group at Michigan State University, headed by Marcos Dantus. When the pulse shaper arrived in St Andrews, it had suffered some damage in transit; one of the mirrors had fallen from its mount and shattered, while others had swivelled in their holders. Therefore, the first task we had to undertake was to replace the broken mirror and realign the pulse shaper.

In the course of our experiments with our microscope systems, we noticed an additional problem with the pulse shaper: the effects of spectral inhomogeneity over the beam's profile, also known as spatial chirp. As the beam was steered, the measured fundamental and SHG spectra after the microscope objective would change. This effect decreased the bandwidth at the sample, which had a potential effect on our experiments. The SHG bandwidth decreased as well, which reduced the wavelength range over which dispersion compensation

was effective. To correct this problem, we adjusted the shaper's alignment once more to correct a slight length difference between the beam's path before and after the shaper's spatial light modulator. After this realignment, the spatial profile was much more uniform.

After the shaper was aligned, we performed initial tests of the MIIPS system by measuring the dispersion of simple systems involving lenses and low-NA objectives, which have less total dispersion than the trapping microscope. The MIIPS method requires the collection of second harmonic light generated by the laser at the sample plane, so we used the 0.05mm thick KDP crystal and UV-grade fused silica collecting lens supplied with the system to generate the SHG signal and couple it into the fibre head of an Ocean Optics USB 4000 spectrometer (see Figure 3.6 for a photo). The orientation of the crystal with respect to the laser's polarisation is critical for generating the widest possible SHG bandwidth, which determines the range over which dispersion can be compensated. Also crucial is the alignment of the SHG collection, especially coupling into the spectrometer.

Although we were able to successfully collect SHG signal and use MIIPS to compensate for objectives with low NA, we were unable to find any SHG signal with 20x or higher magnification microscope objectives. The problem turned out to be the working distance of the objectives; because of the way the supplied KDP crystal was mounted, it was impossible to focus the beam on the crystal surface. Second harmonic generation is a two-photon process, so this focusing was critical. However, the KDP crystal could not be unmounted to allow it to be brought closer to the microscope objective. To solve this problem, we ordered a new crystal (0.1mm BBO, cut to be phase-matched at 800nm) and designed a mount for the crystal so that it is sandwiched between two coverslips. The coverslip facing the objective is of the same material and thickness as those used for the trapping samples, so the dispersion is the same; the coverslip facing the spectrometer is quartz, which has minimal absorption in the UV range covered by the laser's second harmonic. We also designed a SHG collection system that

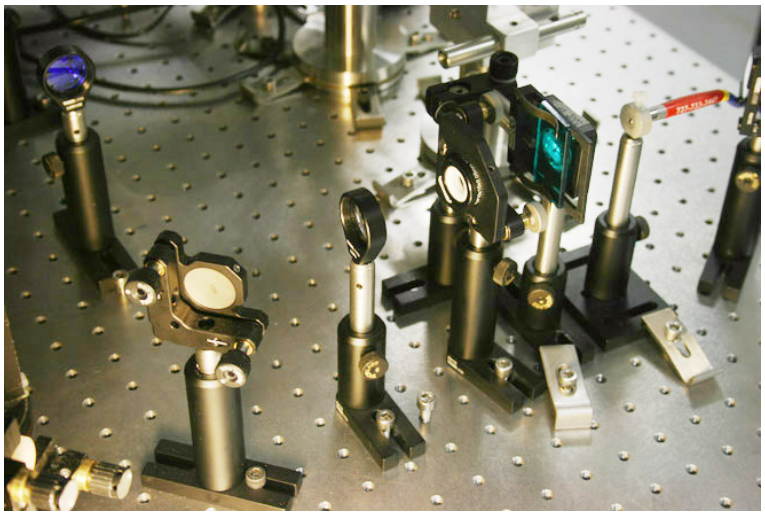

Figure 3.6:
Setup for detection of SHG signal, for systems not including high numerical-aperture (NA) microscope objectives. This is the design that was suggested by BioPhotonic Solutions, Inc. A lens focuses the laser onto a SHG crystal (0.05mm thick KDP). The resulting signal is then filtered to remove the laser's fundamental spectrum, and focused using a 25mm UV-grade fused silica lens onto the fibre collector of an Ocean Optics USB 4000 spectrometer.

could collect more of the SHG generated by a high-NA objective, and would keep the beam, crystal, collection lenses, and fibre collinear.

This SHG collection design for high-NA objectives is shown in Figure 3.7. SHG signal is generated using an 0.1mm thick BBO crystal, cut to be phase-matched for second harmonic generation at 800nm. The crystal is placed in the sample plane after immersion oil and a coverslip identical to those used for the trapping samples. A quartz coverslip protects the top of the crystal; SHG light passes through the coverslip, is collected by a series of two UV-grade fused silica lenses, and is focused on the fibre head of an Ocean Optics USB 4000 spectrometer. A short-pass filter normally prevents the laser's fundamental spectrum from reaching the spectrometer. To collect the laser's fundamental spectrum (needed for calculation of pulse duration at the sample), the short-pass filter is removed and white paper is used as an attenuating scatterer. This SHG collection system is kept rigid and collinear using an optical cage system. When dispersion measurement is finished, the SHG detection portion of the

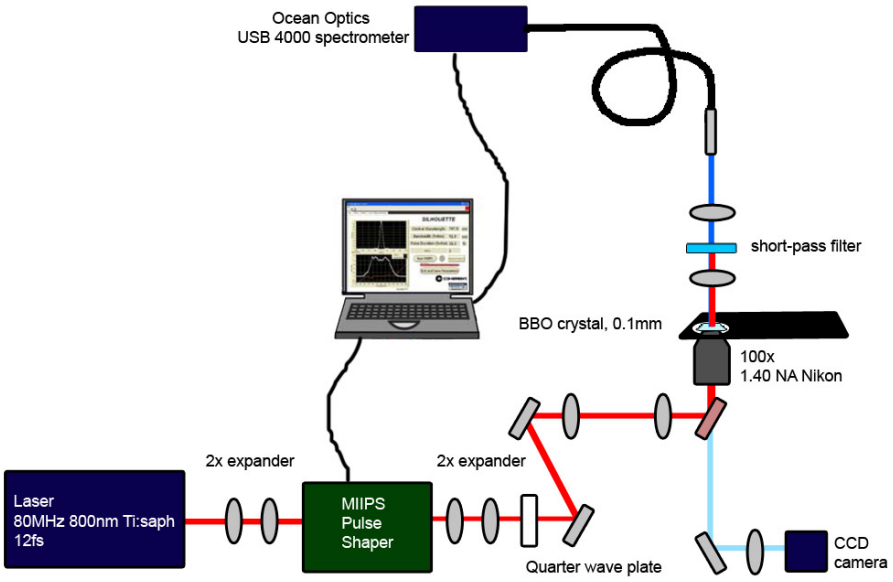

Figure 3.7:
Experimental setup showing collection of second harmonic generation (SHG) light for use in the MIIPS dispersion measurement and compensation method. A thin (0.1mm) BBO crystal is placed in the sample plane, and a series of UV-grade fused silica lenses collects most of the SHG light, focusing it on the fibre head of the spectrometer.

setup is removed and replaced with the QPD position detection (described in Section 3.3).

Most of the experimental work in this thesis was performed with this SHG collection system. Later, a SHG collection unit specifically designed for high NA microscope objectives (Microscope Detection Unit, or MDU) was sent from BioPhotonic Solutions, Inc. This unit was found to work equivalently to my SHG collection system, but was more compact and faster to realign. The MDU is designed only for inverted microscopes, so variants of our own SHG collection design are used in the Bessel beam experiments, which use an upright microscope.

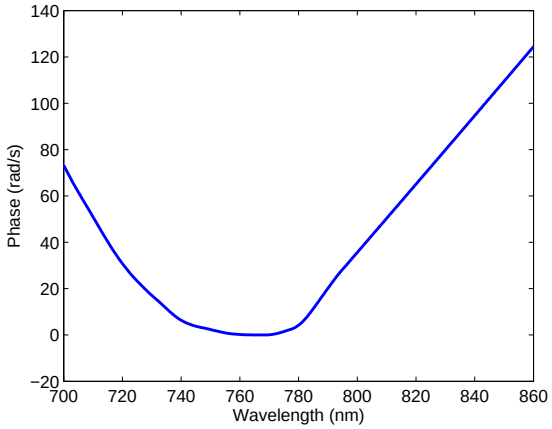

Figure 3.8:
Total measured dispersion of the entire trapping system, including laser and pulse shaper. Note that although dispersion is dominated by a quadratic function (corresponding to GVD, or 2nd order dispersion), there is significant distortion of this curve, indicating the presence of higher-order dispersion as well. This measurement includes not only the trapping microscope but also residual dispersion in the laser cavity, and some slight dispersion introduced by the pulse shaper. It is also possible to calculate the dispersion of the trapping microscope alone, by measuring the dispersion of the system immediately after the MIIPS pulse shaper, and subtracting this from the measured total system dispersion.

3.4.2 Results

Figure 3.8 shows the MIIPS measured dispersion of the entire optical trapping system, including the 100x oil immersion objective. This dispersion, expressed as phase delay as a function of wavelength, is dominated by a quadratic shape, indicating the presence of large amounts of 2nd order dispersion (also known as group velocity dispersion, or GVD). The dispersion contributed by BK7 glass, the vast majority of the dispersive material in the system, is known to be primarily second-order (see Figure 2.2), so this finding comes as no surprise. The quadratic phase delay vs wavelength relationship is modulated by additional distortions, indicating the presence of significant higher-order dispersion. BK7 glass does introduce small amounts of higher-order dispersion; antireflection coatings, dielectric mirrors, the laser cavity, and the shaper itself are also contributors of higher-order dispersion.

Once we measured dispersion, we were able to pre-compensate for it by using the shaper to add the inverse phase vs wavelength function. Note that because we measured higher orders of phase distortion, we were able to compensate these higher orders in addition to 2nd order phase distortion. It has been calculated that with 2nd order dispersion compensation only, the shortest possible pulse duration at the sample plane of a high NA microscope system is around 30fs [27]. By compensating all orders of dispersion we were able to obtain near transform-limited (TL) pulse durations of around 12.9fs FWHM. Some uncompensated residue does remain, particularly at spectral wings where generated SHG signal is weak, but the ratio of compensated pulse duration to theoretical TL pulse duration is less than 1.005.

The dispersion introduced by the microscope system has a dramatic effect on pulse duration at the sample. Figure 3.9 shows the calculated temporal profile of the pulse before (left) and after (right) dispersion compensation. These temporal profiles were calculated using inverse Fourier transform, given the laser's fundamental spectrum and measured spectral phase at the sample. The uncompensated pulse clearly shows the lengthening effects of 2nd order dispersion, as well as the temporally distorting effects of higher order dispersion. These higher order dispersive effects make FWHM pulse duration (based on an assumed Gaussian temporal profile) a less meaningful measure of pulse duration. However, it is evident that dispersion compensation has reduced pulse duration by roughly two orders of magnitude.

The effects of this reduction of pulse duration (and therefore increase in peak power) on nonlinear processes can be clearly seen in Figure 3.10, which shows typical second harmonic signal generated in a BBO crystal by the laser beam at the trapping plane before and after dispersion compensation. To increase the accuracy of compensation, the shaper's grating was translated to produce negative 2nd order dispersion; this had the effect of partially compensating for the positive 2nd order dispersion in the system, decreasing the amount of dispersion the shaper's SLM had to compensate. Without this additional precompensa-

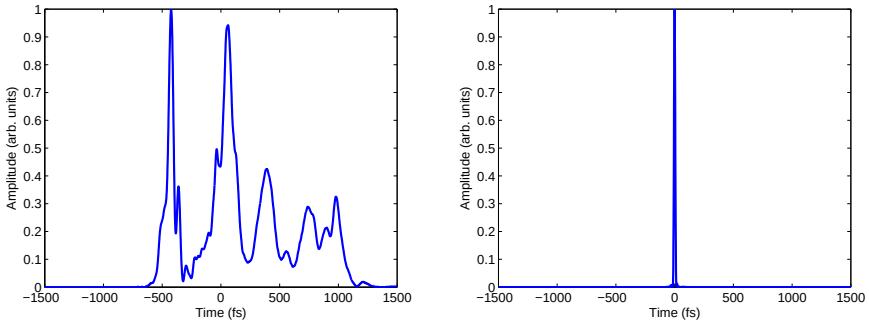

Figure 3.9:
Calculated temporal profile of the pulse at the sample plane before (left) and after (right) dispersion compensation. These calculations were based on the pulse's measured spectral amplitude and phase, using inverse Fourier transform. The FWHM duration of the compensated pulse is 12.9 fs.

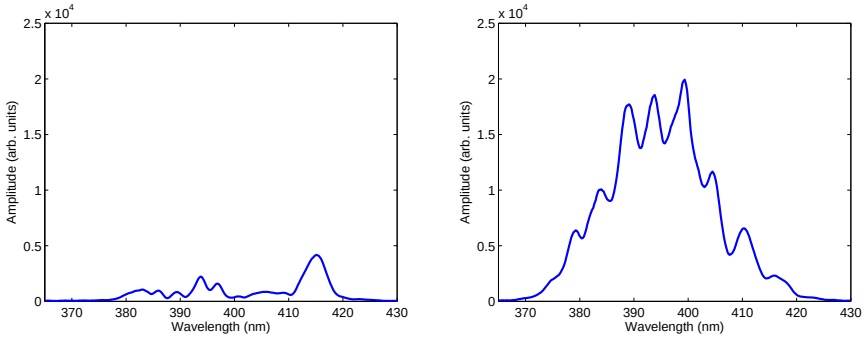

Figure 3.10:
Second harmonic generated using a BBO crystal at the sample plane, before (left) and after (right) dispersion compensation. Note the approximately 740% increase in amplitude, and difference in shape.

tion, the SHG signal before MIIPS compensation would have been even weaker. The same average power was used in both cases, but dispersion compensation has increased the amount of second harmonic generation by about 740%. The uncompensated SHG signal changes from day to day due to slight shifts in the laser cavity alignment, so dispersion compensation also increases reproducibility. A similar increase in efficiency and reproducibility can be expected for other multiphoton processes, such as two-photon excitation.

We have confirmed that the MIIPS method of dispersion measurement and compensation adapts well to our optical trapping microscope; it should be noted

that there are some kinds of dispersion for which this method would not be suited. For example, the pulse shaper applies the same phase function uniformly across the pulse's spatial profile, so it is unable to compensate for dispersion that varies spatially. Although spatially varying dispersion could be measured by collecting SHG signal from different points from the spatial profile, the pulse shaper can only compensate for one of these measured dispersion values at a time. Also, as mentioned in Section 2.2.3, due to hardware limitations, pulse shapers cannot apply phase functions of unlimited magnitude. With the use of additional dispersion pre-compensation such as chirped mirror or prism pairs, this range can be extended, but systems with extreme amounts of dispersion (containing more than a few centimetres of optical fibre, for example) would still prove extremely challenging. Future developments of the MIIPS method may offer solutions to these limitations.

3.5 Conclusion

This chapter described the construction of two optical systems: an optical trapping system, and an axicon system. Both systems share a 12fs pulsed Ti:sapphire laser and a pulse shaper, used to implement the MIIPS method of dispersion measurement and compensation. This chapter focused on the overall setup, and on the construction and dispersion compensation of the optical trapping system, with detailed discussion of the axicon system left for Chapter 5.

At the core of the optical trapping system is a home-built inverted microscope, built according to a design by Phillip Jess. The microscope incorporates a high-NA objective to create the necessary intensity gradient, and a CCD camera for imaging. A monochromator/spectrometer detects fluorescence signals from the sample plane, and was installed with the guidance of Phillip Jess. A white light fibre source illuminates the sample plane, using a design outlined and constructed by Steve Lee. Position detection is implemented by focusing scat-

tered light from the sample plane onto a QPD, also a setup Steve Lee designed and first implemented. A large part of designing the QPD position detection involved overcoming additional alignment considerations imposed by the home-built nature of our microscope system, for example, the significant thickness of the dichroic mirror. This installation therefore required several days and several setup redesigns. Once the scattered light successfully reached the QPD, we installed a data acquisition card and a LabView program, adapted by Steve Lee from a program written by Peter Reece, to read the voltage signals from each of the QPD's quadrants. These voltage time traces are converted to power spectra, from which the trap stiffness is calculated, using a Mathematica program written by Michael Mazilu. Although other programs were available for calculating trap stiffness, including a freely available MatLab program by Tolic-Norrelykke, Hansen, and co-workers [54, 55], the noise level of our system stymied the fitting algorithms of these programs, and necessitated the development of our own program. The resulting system is a flexible optical trapping microscope capable of monitoring the position and emission spectra of optically trapped particles.

To manage dispersion and allow pulse shaping, we aligned and installed a pulse shaper designed by BioPhotonic Solutions, Inc., with the support of Igor Pastirk through telephone and email. A setup of our design collects second harmonic signal from a nonlinear crystal at the sample plane, providing information that the MIIPS algorithm uses for measuring dispersion. Once measured, the dispersion is eliminated by using the pulse shaper to add the inverse dispersion function. Dispersion compensation through high-NA microscope objectives is relatively new[24] and requires extra care in alignment of the pulse shaper and SHG collection optics, as well as being particularly demanding of the MIIPS algorithm. The interplay between alignment and software caused problems with the MIIPS algorithm that occupied many weeks of the time spent on these projects. The eventual identification of the most critical parameters, as well as the arrival toward the end of the year of an SHG collection device from BioPhotonic Solutions, Inc., made the dispersion compensation more consistent and

reliable.

This chapter next showed the temporal profile and SHG spectra before and after dispersion compensation, demonstrating a decrease in pulse duration of approximately two orders of magnitude compared to a system with only partially compensated dispersion, and an approximately 740% increase in SHG signal. We were able to achieve transform-limited 12.9fs pulse durations at the focal plane of the 1.40 NA microscope objective, by far the shortest pulse durations yet available at the sample plane for optical trapping. Additionally the pulse shaper allows a myriad of other temporal, spectral phase, and spectral amplitude functions to be explored with high precision and reproducibility. The effects of pulse shaping on optical trapping, as well as on the emission spectra of optically trapped particles, are discussed in Chapter 4.

The second optical system is used for producing dispersion-compensated axicon-generated Bessel beams. This system is based on an upright microscope designed by Xanthi Tsampoula, and constructed, characterised, and dispersion compensated with her help. The axicon system, and its dispersion compensation by MIIPS, are described in detail in Chapter 5.

Chapter 4

Optical trapping with ultrashort laser pulses

4.1 Introduction

4.1.1 Optical trapping

Optical trapping allows the contact-free manipulation of microparticles by light, fostering applications in a wide array of fields since its introduction by Arthur Ashkin in the 1970s[56, 57]. Particles can be trapped by two counter-propagating beams (dual beam optical trap) or by a single beam (optical tweezers). The sizes of trapped particles can range from tens of microns down to tens of nanometres, with required trapping powers in the range of tens to hundreds of milliwatts. Optical trapping has been used to manipulate a range of particle types, including dielectric particles, metallic particles, living cells, supercooled atoms, and aerosol droplets suspended in air. Optical traps can operate singly or, through the use of technologies such as holographic optical tweezers[5], in parallel by the hundreds. This thesis will focus on the use of single-beam optical tweezers to trap dielectric microspheres whose diameters are comparable to or larger than the wavelength of the trapping beam; this size regime can be described using

Mie scattering.

In the Mie or Lorentz-Mie size regime, the interaction of a dielectric microsphere with a beam of light is governed by transfer of momentum from the incident light to the microsphere as the light is refracted through the sphere (Figure 4.1). As an incident ray of light is refracted through a dielectric sphere, its trajectory changes, meaning that the light has undergone a change in momentum. According to Newton's third law, the sphere experiences an equal and opposite change in momentum, pushing it in the opposite direction from that of the refracted ray.

When an intensity gradient is present in the incident beam, more light rays will impinge on the sphere from the higher-intensity region than from the lower-intensity region - so more rays will refract away from the higher-intensity region than toward this region. Consequently, the net momentum change of the sphere draws it toward the higher-intensity region (Figure 4.1 a). This effect can operate both axially (in the direction of beam propagation) and in the transverse direction (Figure 4.1 b). A focused Gaussian beam has an intensity gradient that points in all directions toward the beam focus. Therefore the sphere is trapped at the beam focus, and experiences a spring-like restoring force that draws it back toward the beam focus whenever Brownian motion or outside forces perturb its position.

The Mie regime interaction of a dielectric sphere with incident light can be modelled using Mie scattering, which is based on ray optics. In Mie scattering, the force on a dielectric sphere is decomposed into a scattering force (in the direction of beam propagation) and a gradient force. Each incident ray of light applies a force on the sphere, depending on its incident angle θ_i and its power P. Components of the incident ray are reflected or refracted according to Fresnel reflection and transmission coefficients. The expression for the total force exerted by the incident ray requires the summation of momentum changes due to an infinite number of refracted rays arising from multiple internal reflections. Ashkin's calculations [59] give the exact expression for the scattering force (F_s)

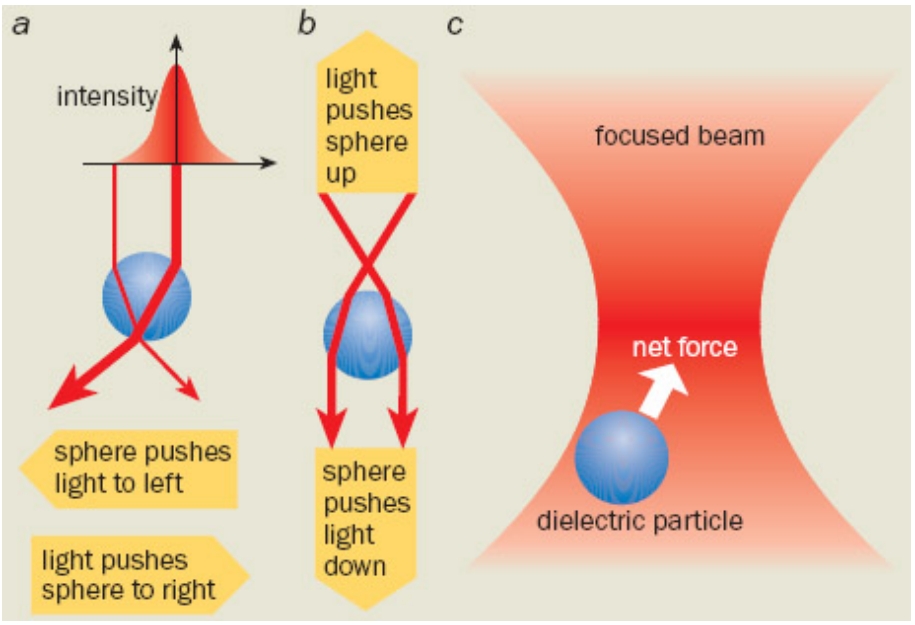

Figure 4.1:
Figure is from [58]. This cartoon illustrates how the transfer of momentum in the Mie regime draws a dielectric microparticle toward the highest-intensity area of a focused Gaussian beam. a) When the particle is located to the left of the highest-intensity area, more rays impinge on the particle from the right than from the left, so more light is pushed to the left. As a result, the particle moves to the right, toward the highest-intensity area. b) When the sphere is located below the highest-intensity area, the rays that are refracted through the sphere experience a momentum change in the downward direction. Consequently, the sphere is pushed in the upward direction, towards the highest-intensity area. c) In a focused Gaussian beam, the intensity gradient points toward the beam focus, so the sphere is drawn toward the beam focus.

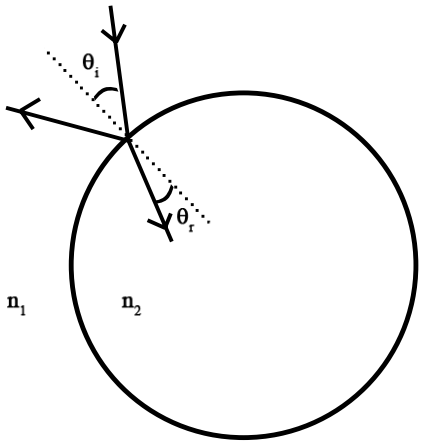

Figure 4.2:
Sketch after [59] showing geometry for calculating the scattering and gradient force on a dielectric microsphere due to a single ray incident at angle θ_i. The medium has refractive index n_1 and the sphere has refractive index n_2. Only the first refraction is shown here; in reality the refracted ray undergoes an infinite series of reflection/refraction events as it careens through the sphere interior, all of which must be taken into account in the final calculation.

and gradient force (F_g) due to this single incident ray as:

$$\begin{aligned} F_s &= \frac{n_1 P}{c}\left[1 + Rcos2\theta_i - \frac{T^2\left[cos(2\theta_i - 2\theta_r) + Rcos2\theta_i\right]}{1 + R^2 + 2Rcos2\theta_r}\right] \\ F_g &= \frac{n_1 P}{c}\left[Rsin2\theta_i - \frac{T^2\left[sin(2\theta_i - 2\theta_r) + Rsin2\theta_i\right]}{1 + R^2 + 2Rcos2\theta_r}\right] \end{aligned}$$

where R and T are the calculated Fresnel reflection and transmission coefficients for the ray incident at angle θ_i to the normal and refracted at angle θ_r (Diagram in Figure 4.2). The refractive index of the medium is n_1. To calculate the total force on the sphere due to all incident rays, the contributions of each ray must be summed up, allowing for the beam's intensity gradient and the sphere's location.

The effects described above are not time-dependent (more discussion in Section 4.2), and therefore allow the particle to be trapped by a time-varying (for example, pulsed) beam[7]. The pulse repetition rate must be high enough that the particle does not diffuse significantly between pulses. In this work, a laser

with 80MHz repetition rate is used, which satisfies this condition. Optical trapping using pulsed lasers will be introduced in Section 4.1.2 below, and will be the subject of theoretical and experimental work in the remainder of this chapter.

4.1.2 Pulsed lasers in optical trapping

The high peak powers of pulsed lasers have made them attractive to many researchers for use in optical trapping, whether as trapping beams or as probe beams in combination with continuous-wave (CW) trapping beams. Pulsed lasers offer extremely high peak powers at lower average powers, allowing efficient access to multiphoton processes that would otherwise require enormously high average powers.

Previous research in pulsed optical tweezing has demonstrated some of these multiphoton processes in optically trapped particles. Using a CW trapping beam in combination with a pulsed nanosecond laser, Misawa and co-workers observed multiphoton ablation and self-focusing in trapped latex spheres[10]. Using pulsed femtosecond lasers as the trapping beam, Malmqvist and co-workers studied second harmonic generation (SHG) in optically trapped Rayleigh-sized KTP and $LiNbO_2$ particles[8], while Agate and co-workers studied two-photon excitation in optically trapped dyed polymer particles in the Mie and Lorentz-Mie regime[7]. Perevedentseva and co-workers observed SHG in biotin and biotin ester microcrystals trapped by a pulsed laser[9]. Researchers have also used two-photon excitation in fluorescein medium surrounding optically trapped particles to study optical binding[60, 61]. Morrish and co-workers have studied morphology-dependent resonances induced by two-photon excitation in optically trapped particles[62, 13]. Fontes and co-workers studied two-photon morphology-dependent resonances, hyper-Raman, hyper-Rayleigh, and two-photon excitation in trapped particles (as well as linear effects)[12]. Coherent anti-Stokes Raman scattering in trapped particles was studied by Chan and co-workers[11]. Kuriakose and co-workers studied two-photon morphology-dependent resonances in particles trapped by a femtosecond near-field optical trap[63].

In addition to multiphoton excitation, pulsed lasers have also been studied for their effects on the trapping process itself. The multiphoton effects caused by highly-focused lasers can have harmful effects in trapped cells[64], so researchers have proposed a method to corral cells without damage using another nonlinear effect of pulsed lasers, shock waves from cavitation[65]. A closely related commonly-used technique, Laser Microdissection and Pressure Catapulting (LMPC) uses cavitation shock waves from pulsed lasers as a noninvasive method for levitating cells[66].

Another method for manipulating particles using pulsed lasers was executed at cryogenic temperatures, where a femtosecond pulsed laser was used to guide semiconductor nanoparticles of radius as little as 10nm along the laser beam to a target a few centimetres away[67]. The guiding was only found to work when the pulse wavelength was tuned to be resonant with excitronic transitions in the particles.

The peak powers of pulsed laser sources have also been used in separating stuck particles from surfaces. This phenomenon was theoretically modelled in a paper by Deng et al[68], who calculated that the peak gradient force during a laser pulse was enough to overcome the binding interaction between a stuck particle and the surface. Ambardekar et al used a microsecond pulsed laser to separate stuck 2μm polystyrene beads and yeast cells from their substrates[69], which they attributed to the high peak gradient force of their pulsed laser.

Pulsed lasers also have been reported to produce enhanced lateral optical trapping in Rayleigh-sized particles, while creating extraordinarily high axial forces. Pan et al optically trapped clumps of 3-4nm quantum dots using a picosecond pulsed laser source of 120-140mW average power, and calculated that this trapping would be not be possible in a CW source of less than 20W power[70]. They attributed the success of the optical trapping to the ability of pulsed lasers to apply their trapping force over a very short timescale, during which the particle's Brownian motion would not carry it significantly away from the focus. Related papers by another research group explored theoretically

the trapping of Rayleigh-sized particles with pulsed lasers and calculated an extremely high peak force [71], although they did not examine average force over a pulse's repetition cycle. They calculated that neither Brownian motion nor gravity would cause a 5nm particle to diffuse significantly between pulses if the repetition rate were above 100Hz. Their calculations indicated no major material dependence or wavelength dependence. In an earlier paper on a very different size scale, Misawa et al also observed guiding of pyrene-doped polymer (7.2μm diameter) in the axial direction during irradiation with a pulsed laser, but observed this guiding in combination with laser ablation of the polymer[10].

To date the only experimental comparison of the trapping force for a CW source and a pulsed femtosecond laser of the same average power is reported in a 2004 paper by Agate et al[7]. They found no difference in trap stiffness between the CW and the pulsed laser source, for 1.28μm silica spheres.

As seen in the examples above, the high peak powers of pulsed lasers allow access to material-dependent or medium-dependent nonlinear processes, some of which can have significant effects on optical trapping, guiding, or other mechanical laser micromanipulation. It is less clear whether there are material-independent optical trapping effects that depend on peak power rather than average power; that is, whether pulsed lasers behave differently from CW lasers in optical trapping. If optical trapping is independent of the laser's temporal/phase characteristics, then it should be possible to use advanced pulse shaping methods for spectroscopic techniques on trapped particles, without affecting the trapping process itself. This chapter seeks to address these questions through theory, simulation, and experiment. In section 4.2, Mie scattering theory is used to calculate whether optical trapping using pulsed lasers is phase-dependent; that is, whether the pulse duration of the trapping source has an effect on the average force applied to a trapped particle. In section 4.3, an experimental investigation of trap stiffness as a function of pulse duration is carried out using a dispersion-compensated femtosecond laser source and silica particles of 780nm diameter. Finally, section 4.4 demonstrates the control of multiphoton

excitation in optically trapped polystyrene particles using phase shaped ultrashort pulses, demonstrating the possibility of advanced spectroscopy methods in trapped particles.

4.2 Theoretical analysis using Mie scattering

This section outlines theoretical arguments demonstrating that optical trapping does not depend on the duration of a pulsed laser, but only on the laser's frequency spectrum. In other words, trapping with a pulsed laser source should be equivalent to trapping with a CW laser source with the same bandwidth and average power. Here, we assume that pulse repetition rate is high enough that the particle does not diffuse significantly between pulses; for very low (less than around 1kHz) repetition rates, the time profile will play a role. We also assume that scattering is not frequency-dependent.

Below I detail arguments that were outlined by a co-researcher, Michael Mazilu.

Consider a laser pulse whose electric and magnetic fields $\boldsymbol{\mathcal{E}}(x,y,z,t)$ and $\boldsymbol{\mathcal{H}}(x,y,z,t)$ are both position-dependent and time-dependent. Assuming that each x,y,z position within the laser pulse has the same time dependence, and that the electric and magnetic fields have the same time dependence, we can decompose the pulse into separate position and time dependencies:

$$\boldsymbol{\mathcal{E}}(x,y,z,t) = \mathbf{E}(x,y,z)a(t) \tag{4.1}$$

$$\boldsymbol{\mathcal{H}}(x,y,z,t) = \mathbf{H}(x,y,z)a(t) \tag{4.2}$$

Write the time dependencies in their frequency domain form (by taking the Fourier transform):

$$\boldsymbol{\mathcal{E}}(x,y,z,t) = \mathbf{E}(x,y,z)\int \hat{a}(\omega)e^{-i\omega t}d\omega \tag{4.3}$$

$$\boldsymbol{\mathcal{H}}(x,y,z,t) = \mathbf{H}(x,y,z)\int \hat{a}(\omega)e^{-i\omega t}d\omega \tag{4.4}$$

Here, $\hat{a}(\omega)$ is the Fourier transform of $a(t)$. Now that we have our pulse, we need to calculate its effect on the particle. The electromagnetic force density

$$f_i = \partial_j T_{ij} - \partial_t g_i \tag{4.5}$$

gives us the amount of force exerted by the laser pulse's electromagnetic field in an infinitesimally small volume within the particle, at a given point in time[1][2][72, 73]. f_i is made of two terms, both dealing with momentum transfer from the pulse to the particle (as evidenced by a change in momentum or in momentum density). The first term comes from the influx of momentum

$$T_{ij} = \mathcal{E}_i\mathcal{D}_j + \mathcal{H}_i\mathcal{B}_j - \frac{1}{2}\delta_{ij}(\mathcal{E}_k\mathcal{D}_k + \mathcal{H}_k\mathcal{B}_k) \tag{4.6}$$

and the second term arises from the variation in electromagnetic momentum density

$$g_i = \epsilon_{ijk}\mathcal{D}_j\mathcal{B}_k \tag{4.7}$$

Here, $\mathcal{D}_i = \epsilon_r\epsilon_0\mathcal{E}_i$ (electric displacement), and $\mathcal{B}_i = \mu_r\mu_0\mathcal{H}_i$ (magnetic flux). ϵ_r is the relative dielectric constant, ϵ_0 is the permittivity of free space, μ_r is the relative permeability, and μ_0 is the permeability of free space. ϵ_{ijk} is the Levi-Civita antisymmetric tensor. [3]

[1] Here,

$$\begin{aligned} i &= 1,2,3 \\ j &= 1,2,3 \\ k &= 1,2,3 \end{aligned}$$

are indexes corresponding to the directions in each of the 3 Cartesian coordinates. That is, $T_{11} = T_{xx}$, $T_{12} = T_{xy}$, $T_{13} = T_{xz}$, etc.

[2] We write these expressions in compact form using Einstein summation convention. In this convention, writing $\partial_j T_{ij}$ is equivalent to writing $\sum_{j=1,3}\partial_j T_{ij} = \partial_x T_{ix} + \partial_y T_{iy} + \partial_x T_{iz}$

[3] This is a completely antisymmetric tensor of 3rd rank, defined by

$$\epsilon_{123} = \epsilon_{231} = \epsilon_{312} = 1$$

$$\epsilon_{213} = \epsilon_{321} = \epsilon_{132} = -1$$

$$\epsilon_{ijk} = 0\ otherwise$$

To calculate the total optical force exerted by the pulse on the entire particle, over the entire duration of the pulse, we need to integrate equation 4.5 over the particle's volume, and over time. So that we may discuss the answer in terms of average force exerted, instead of assuming a single pulse and integrating from $-\infty$ to $+\infty$, we assume a train of pulses where the pulse repetition period τ is much larger than the pulse duration. The momentum density g_i term of f_i cancels out during this averaging:

$$\int_0^\tau \partial_t g_i dt = g_i(\tau) - g_i(0) \tag{4.8}$$

and $g_i(\tau) = g_i(0)$ since there is no field at time 0 and τ. We are left with an expression for the average optical force that contains only the T_{ij} term:

$$\begin{aligned} < F_i > &= \frac{1}{\tau}\int_0^\tau f_i dV dt & (4.9)\\ &= \frac{1}{\tau}\int_0^\tau \oint T_{ij} ds_j dt & (4.10) \end{aligned}$$

The second equation includes a surface integral evaluated on a closed surface surrounding the particle, with $ds_j = n_j ds$ being a unit vector normal to the surface. Inserting equation 4.6 into equation 4.10 gives us

$$\begin{aligned} F_i &= \frac{1}{\tau}\oint\int_0^\tau T_{ij} dt ds_j & (4.11)\\ &= \frac{1}{\tau}\oint\int_0^\tau \left[\mathcal{E}_i\mathcal{D}_j + \mathcal{H}_i B_j - \frac{1}{2}\delta_{ij}(\mathcal{E}_k\mathcal{D}_k + \mathcal{H}_k\mathcal{B}_k)\right] dt ds_j & (4.12)\\ &= \frac{1}{\tau}\left[\oint\int_0^\tau \mathcal{E}_i\mathcal{D}_j dt ds_j + \oint\int_0^\tau \mathcal{H}_i\mathcal{B}_j dt ds_j + \ldots\right] & (4.13) \end{aligned}$$

Examine the first term in equation 4.13 (similar arguments will hold for all

the other terms). Using equation 4.3, this term can be rewritten as

$$\begin{aligned}
\oint \int_0^\tau \mathcal{E}_i \mathcal{D}_j dt ds_j &= \epsilon_r \epsilon_0 \oint \int_0^\tau \mathcal{E}_i \mathcal{E}_j dt ds_j \\
&= \epsilon_r \epsilon_0 \oint \int_0^\tau E_i \int \hat{a}(\omega_1) e^{-i\omega_1 t} d\omega_1 E_j \int \hat{a}(\omega_2) e^{-i\omega_2 t} d\omega_2 dt ds_j \\
&= \epsilon_r \epsilon_0 \oint E_i E_j \int_0^\tau \iint \hat{a}(\omega_1)\hat{a}(\omega_2) e^{-i(\omega_1+\omega_2)t} d\omega_1 d\omega_2 dt ds_j \\
&= \epsilon_r \epsilon_0 \oint E_i E_j \iint \hat{a}(\omega_1)\hat{a}(\omega_2) \left[\int_0^\tau e^{-i(\omega_1+\omega_2)t} dt \right] d\omega_1 d\omega_2 ds_j
\end{aligned}$$

Now using our earlier assumption that the time Δt between pulses is very long, we can use a property of Dirac delta functions

$$\int_{-\infty}^{+\infty} e^{-i\omega t} dt = \delta(\omega) \tag{4.14}$$

to simplify further:

$$\begin{aligned}
\oint \int_0^\tau \mathcal{E}_i \mathcal{D}_j dt ds_j &= \epsilon_r \epsilon_0 \oint E_i E_j \iint \hat{a}(\omega_1)\hat{a}(\omega_2) \left[\delta(\omega_1+\omega_2)\right] d\omega_1 d\omega_2 ds_j \\
&= \epsilon_r \epsilon_0 \oint E_i E_j \int \hat{a}(\omega_1) \left[\int \hat{a}(\omega_2)\delta(\omega_1+\omega_2) d\omega_2 \right] d\omega_1 ds_j
\end{aligned}$$

And using the definition of Dirac delta functions,

$$\int f(t)\delta(t-t_0)dt = f(t_0) \tag{4.15}$$

we eliminate one of the integrals to get

$$\oint \int_0^\tau \mathcal{E}_i \mathcal{D}_j dt ds_j = \epsilon_r \epsilon_0 \oint E_i E_j \int \hat{a}(\omega_1)\hat{a}(-\omega_1) d\omega_1 ds_j \tag{4.16}$$

$$= \epsilon_r \epsilon_0 \oint E_i E_j \int \hat{a}(\omega_1)\hat{a}^*(\omega_1) d\omega_1 ds_j \tag{4.17}$$

($\hat{a}(\omega_1) = \hat{a}^*(-\omega_1)$ because $a(t)$ is real.) Note that $\hat{a}(\omega_1)$, the laser's spectrum,

is multiplied by its complex conjugate, eliminating any contributions from the laser's spectral phase. This means that the $\mathcal{E}_i\mathcal{D}_j$ term of equation 4.12 depends only on the magnitude of the laser pulse's spectrum, not on its phase. Following the same arguments, the other terms of equation 4.12 for the average force exerted by the laser pulse also have no phase dependence. Therefore, the spectral phase (or temporal shape or duration) of the pulse does not affect the average optical trapping force. These conclusions are supported by numerical simulations performed by Michael Mazilu, and by the experimental work presented below.

In these arguments, our primary interest has been to determine whether pulse duration has any material-independent effect on optical trapping. We have therefore made a few assumptions about material properties such as refractive index, which are valid for the majority of materials, but to which interesting exceptions might be found.

We assumed, for example, that scattering is not frequency-dependent; that is, $n(\omega)$ is effectively constant over the pulse's bandwidth. If a material could be found for which $n(\omega)$ varied by a significant amount, then the bandwidth of the pulse would have an effect on trapping - this effect would not show up in our system, where we vary pulse duration while keeping bandwidth constant, but would be noticeable if an ultrashort system with 100nm bandwidth were compared to a longer-pulsed system with 10nm bandwidth.

We also have assumed a refractive index that is relatively low. For very high-index materials, it is possible that the particles could form optical cavities containing whispering-gallery modes whose resonances are strong enough to affect scattering and therefore optical trapping. This is again an effect that is dependent on bandwidth, and might also be observed when comparing broadband and narrowband CW sources.

One peak power-dependent effect that might be observable in materials with high n_2 is the optical Kerr effect, in which the refractive index (and therefore optical trapping) changes depending on the intensity of illumination. The

extremely high peak powers achievable by our dispersion-compensated pulses might make the Kerr effect noticeable for certain materials.

A material containing significant amounts of optical gain might also display pulse duration-dependent trapping behaviour. The presence of optical gain corresponds to a change in the imaginary part of the material's refractive index, so via the Kramers-Kronig relations, the real part of the refractive index must change as well. If there is enough gain, the change in refractive index might detectably affect trapping.

Another possible material-dependent effect is that of optical damage to the trapped particle. Although we did not observe these effects in the silica particles we used for our investigations of optical trapping forces, in Section 4.4 we describe visible pulse duration-dependent and power-dependent damage observed in polystyrene. This damage occurs along with a change in particle trapping position, with the particles often ejected from the trap altogether. A similar effect was observed by Misawa and co-workers[10]. Some of these special cases may make interesting topics for future investigation.

4.3 Experimental investigation of trap stiffness vs pulse duration

4.3.1 3D optical trapping using a 12.9fs dispersion-compensated pulsed laser

The experiments described in this section are also detailed in a recent publication[74]. Our experimental investigation of the behaviour of ultrashort laser pulses as trapping beams used the optical trapping system described in Chapter 3. This system consists of a 12fs pulsed Ti:Sapphire laser source, a pulse shaper, an inverted trapping microscope with back focal plane position detection, and a spectrometer. We compensated for all orders of dispersion in the system, as described in Section 3.4. The transform-limited (dispersion compensated) pulse

duration at the sample depended on the laser bandwidth that reached the sample. Due to day-to-day fluctuations in cavity alignment that varied this bandwidth, the transform-limited pulse duration at the sample ranged from 11fs-16fs. The experiments described below were performed with 12.9fs FWHM duration dispersion compensated pulses.

To verify 3D optical trapping with our dispersion compensated 12.9fs pulses, we prepared a sample of 780nm diameter silica microspheres, diluted in deionised water. Silica was chosen as the trapping material because it could withstand the dispersion-compensated peak powers at the average powers needed for trapping with a trap stiffness high enough to be accurately measured. At these average powers, polymer was violently ablated (an effect almost identical to that observed by Misawa and co-workers [10]) and gold produced cavitation.

In choosing the optimum particle diameter for our experiment, we had to take into account certain experimental limitations. The ideal experiment would have investigated particle sizes ranging from the Rayleigh regime (diameter $d \ll \lambda$) to the Mie regime ($d \gg \lambda$). However, the maximum power available (47 mW at the sample plane), limited the strength of the trap so larger and smaller particles could not be trapped as easily. Noise also played a role, as the setup suffered from both intermittent and constant noise that produced spikes in the power spectra, making curve fitting difficult for weaker traps. The material damage considerations detailed above forced us to use silica for these experiments rather than polystyrene or gold which would have given us a stronger scattered signal and/or higher trap stiffness values. Consequently, although we were able to detect the accumulation of Rayleigh-regime 50nm and 100nm particles in the trap, the weak trap stiffness and system noise were such that we could not detect single trapped particles. Similarly, although we could trap 2μm silica particles at low powers without damage, the trapping was relatively weak, and noise prevented us from fitting the power spectra well. We therefore chose 780nm as an intermediate particle diameter that would give us the most reliable trap stiffness data.

We measured and compensated the trapping system's dispersion on the same day that these data were taken, to account for day-to-day dispersion fluctuations in the laser cavity. These fluctuations were enough to stretch the pulses by 50fs or more.

We trapped the silica particles at the focus of the laser beam, with an average power at the sample plane of 47mW, measured using the double-objective transmission method [75]. For a diagram of this setup, see Figure 4.3. In this method, the power P_{in} is measured at the back aperture of the objective. The objective is replaced with an iris whose diameter is equal to the diameter of the objective's back aperture, and another measurement $P_{aperture}$ is taken. Then, the iris is removed and the microscope objective replaced, and a coverslip is placed in the sample plane along with the usual microscope objective oil. A second drop of objective oil is placed on a coverslip, and a second microscope objective (identical to the first) is aligned such that the light passing through the sample will be coupled through this microscope objective. Correct xy position is verified by the presence of a circular beam travelling straight upwards through the back aperture of the second objective; the z position is then adjusted such that this beam is collimated (since the objective is infinity corrected). A power meter measures the transmitted power P_{trans} through this second microscope objective. From these measurements, the power at the sample plane can be calculated using

$$P_{sample} = P_{in}\sqrt{\frac{P_{trans}}{P_{aperture}}} \tag{4.18}$$

The sample was diluted enough that only a single particle was trapped at a time, which we confirmed by imaging the sample with a CCD camera (Figure 3.4). The trapping distance was 14μm from the bottom coverslip, measured by bringing a trapped particle toward the bottom coverslip until trapping was no longer observed.

The positions of the trapped silica particles were monitored over 6.7 consecutive seconds at an acquisition rate of 30,000 samples/second for each of the

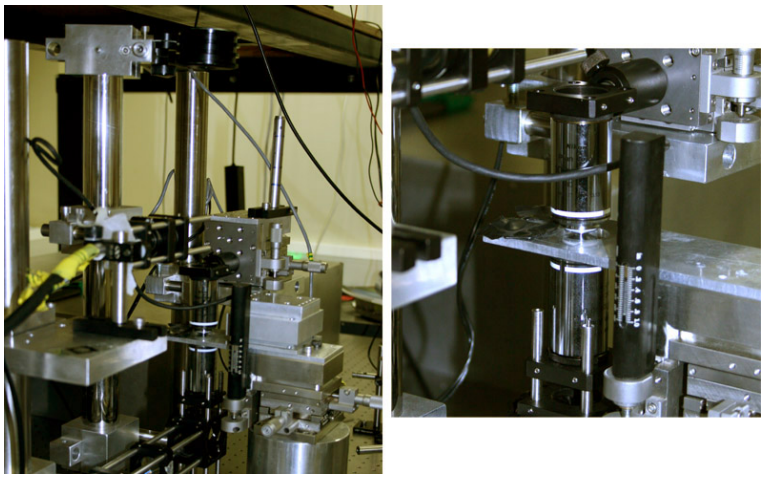

Figure 4.3:
Double microscope objective method for determining power at the sample plane[75]. Left: measuring power after the second microscope objective (power meter is at top centre). Right: zoomed-in view of coverslip/objective oil coupling.

four quadrants of the QPD. This position measurement was repeated six consecutive times for each of three different silica particles (giving a total combined acquisition length of 40 seconds for each particle). We used our own Mathematica program (written by Michael Mazilu) to calculate the power spectra in x, y, and z of each 40 second acquisition and fit a Lorentzian curve to these power spectra. These power spectra and fit for one of the trapped silica particles is shown in Figure 4.4. The cutoff frequency of the fitted Lorentzian curve was then used to calculate the trap stiffness, as described in Section 3.3.

The power spectra indicate stable trapping in 3D by the 12.9fs pulsed laser, which we visually confirmed by translating the sample stage in x, y, and z. We calculate an average trap stiffness of 0.1094±0.009 pN/nm in the x-direction, 0.1204±0.008 pN/nm in the y-direction, and 0.0216±0.008 pN/nm in the z-direction. These values are roughly comparable to the 0.03148 pN/nm lateral trap stiffness values reported in [53] for 15mW average power and slightly different laser wavelength and particle diameter.

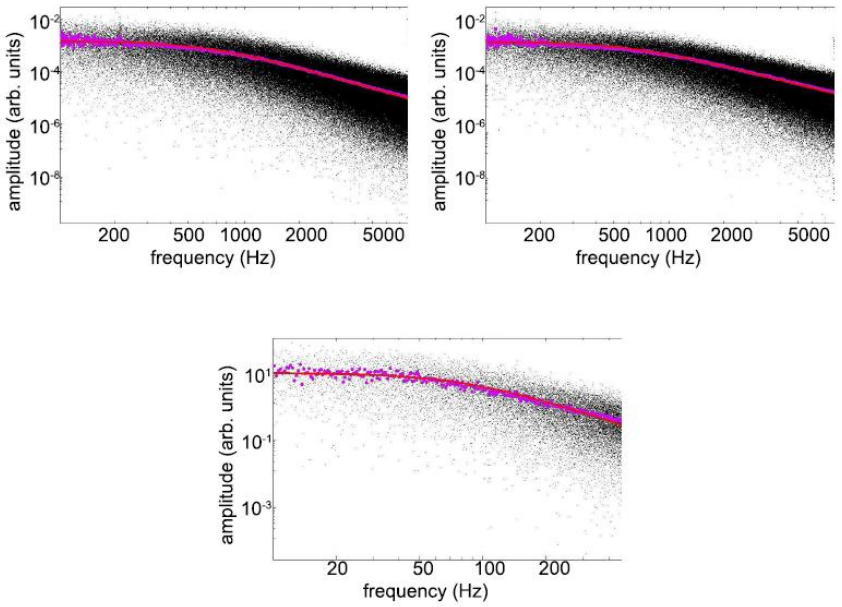

Figure 4.4:
Power spectra of a trapped 780nm silica sphere in x, y, and z directions (upper left, upper right, and bottom, respectively). These power spectra were calculated from a 40 second acquisition at an acquisition rate of 30,000 samples/second; the raw (unbinned) data are shown as black points. The particle was trapped with 47mW average power using dispersion-compensated 12.9fs pulses at 80MHz repetition rate. We fit Lorentzian curves to these power spectra; the experimental data were first binned in logarithmic space to speed the fitting algorithm. The data points resulting from logarithmic binning are shown in purple, while the fitted Lorentzian curves are shown in red. To equally weight the low and high frequencies when fitting, we chose a fitting range that would centre the cutoff frequency along the frequency axis in log-log space. The x and y axes are fit from 100Hz - 8000Hz, while the z axis (with lower cutoff frequency) is fit from 10Hz - 500Hz.

4.3.2 Trap stiffness vs pulse duration

We measured trap stiffness as a function of pulse duration for 780nm diameter silica particles. The optical trapping was performed as described in Section 4.3.1, with single 780nm particles trapped in the pulsed laser beam at 47mW at the sample plane. Trapping was monitored using a quadrant photodiode (QPD) position sensing setup; from the power spectrum of the particle's detected motion within the trap, the trap stiffness was calculated as described in Section 4.3.1.

To control the duration of the laser pulses, we first had to eliminate the existing dispersion on the system. This was done by measuring the dispersion of the entire microscope system using MIIPS, and adding the inverse of this dispersion using the pulse shaper, achieving a net dispersion of zero at the sample. Dispersion measurement and compensation of the optical trapping system is described in Section 3.4.2. This measurement had to be repeated daily, sometimes multiple times daily, to compensate for changing dispersion in the laser cavity, or to adapt to any added or removed optics in the microscope system.

Starting from the clean slate created by dispersion compensation, we stretched the pulses by adding a custom phase function in the shaper, in addition to the phase function that compensated dispersion. The most straightforward method of stretching the pulse is to add positive or negative 2nd order dispersion (also known as GVD, or a quadratic phase function). The advantage of using 2nd order dispersion to increase pulse duration is that the time profile is stretched without changing shape; likewise, the efficiency of multiphoton excitation is decreased monotonically for all wavelengths. We chose to use positive rather than negative 2nd order dispersion because in combination with the mostly negative 2nd order dispersion-compensating phase function, the total magnitude of the phase function created by the SLM is decreased rather than increased. To compensate for the dispersion introduced by the microscope, the SLM was already near the limit of the largest phase function that could be reliably produced; in-

$\gamma_2(\text{fs})^2$	Duration (fs)	Time-bandwidth product
0	12.9	0.66
96	20.0	1.02
117	30.0	1.53
180	50.2	2.56
242	70.0	3.57
337	99.9	5.09
625	200.0	10.20
1530	500.2	25.52

Table 4.1:
Amount of 2nd order dispersion used to produce desired pulse durations. The phase functions used are of the form $\phi(\omega) = \frac{1}{2}\gamma_2(\omega - \omega_0)^2$, where where γ_2 is the amount of 2nd order dispersion in fs^2, and ω_0 is the centre frequency of the phase function. Here, ω_0 is $2.48 * 10^{15}$ rad/s . The resulting FWHM pulse duration (assuming a roughly Gaussian time profile) is calculated using inverse Fourier transform. For the time bandwidth product calculation, the spectral bandwidth is calculated by fitting a Gaussian curve to the spectrum measured at the microscope plane and centred at 780nm, yielding a FWHM bandwidth of 103.8nm.

creasing the magnitude of the phase function by additional negative 2nd order dispersion would have caused unwanted wrapping-related artifacts. Note that if pulse duration had been controlled by changing the spacing of a prism pair in a precompressor, unwanted 3rd order dispersion would have been introduced along with the desired 2nd order dispersion, changing the time profile and the wavelength dependence of multiphoton excitation.

We calculated the pulse durations resulting from various amounts of 2nd order dispersion using inverse Fourier transform, given the test phase function and the fundamental spectrum of the laser. We chose 2nd order dispersion amounts that would produce pulse durations approximately evenly spaced in log scale; these phase functions are of the form $\phi(\omega) = \frac{1}{2}\gamma_2(\omega - \omega_0)^2$, where γ_2 is the amount of 2nd order dispersion in fs^2, and ω_0 is the centre frequency of the phase function. In our case, ω_0 was chosen to be $2.48*10^{15}$ rad/s (corresponding to $\lambda_0 = 759.11nm$). Table 4.1 below shows the γ_2 used, along with the resulting pulse durations.

We introduced these 2nd order phase functions using the pulse shaper and for each pulse duration measured trap stiffness of a trapped 780nm silica particle.

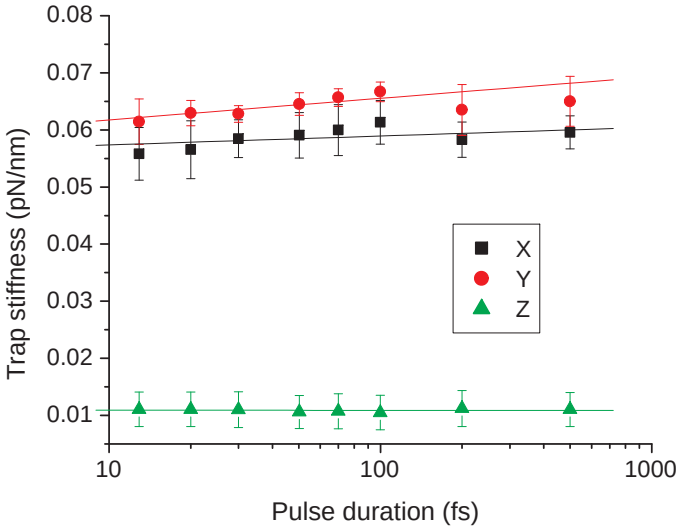

Figure 4.5:
Measured trap stiffness of 780nm diameter silica particles in the x, y, and z directions, trapped in 3D using a pulsed 780nm Ti:Sapphire laser. Each data point shows the average of a 40 second acquisition for each of three trapped particles. Pulse duration was varied from 12.9fs to 500fs using positive 2nd-order phase modulation in addition to a phase function that compensated the measured dispersion on the system. For all measurements, the average power at the sample plane was 47mW. The lines shown are linear fits in log space. The best fit slopes are (in pN/cm per decade): x: 0.00154 ±0.00097, y: 0.00378±0.00133, z: -1.12E-5±1.97E-4.

As in Section 4.3.1, we trapped the particles at 47mW average power, and measured their positions over 6.7 consecutive seconds at an acquisition rate of 30,000 samples/second for each of the QPD's four quadrants. This position measurement was repeated six times for a total acquisition length of 40 seconds for each particle. We repeated this measurement for three particles, and the average trap stiffness in x, y, and z for these three trials is shown in Figure 4.5.

From Figure 4.5, it is evident that although pulse duration was changed by roughly 1.5 orders of magnitude, trap stiffness remained unchanged to within 9%. Trap stiffness in the x and y (transverse) directions increased slightly, but this increase is very close to the fit error. Trap stiffness in the z (axial) direction was unchanged within experimental error. Average power remained the same in

all cases. This observation indicates that in the absence of material-dependent effects, optical trapping in x, y, and z depend on average power rather than peak power.

Some of the 9% variation in trap stiffness can be attributed to slight changes in beam power and spatial profile as the pulse shaper applied different phase functions to the laser. Although ideally there would be no change in beam profile, the large amounts of wrapping in the phase functions, produced as the shaper tried to compensate for the extremely dispersive optical system, produced slight but noticeable intensity changes. These effects limited the range over which we could vary pulse duration; when not compensating for high-NA objectives, the shaper can more accurately implement a wide range of pulse durations.

The above experiments were performed using Lorentz-Mie-sized particles. We attempted to trap Rayleigh-sized particles (50nm and 100nm silica), but were unable to trap single particles at our maximum available average power (47mW). However, at higher particle concentrations we were able to observe gradual accumulation of 50nm and 100nm particles in the trap, indicating the presence of an aggregation/binding effect for small particles. Similarly, the recently-reported accumulation of Rayleigh-sized quantum dots in an optical trap may not be caused by the use of a pulsed laser source, but rather may be due to the trapping of multiple rather than single quantum dots[70].

The absence of a trapping dependence on pulse time profile gives us the freedom to modulate ultrashort pulses to control multiphoton effects in trapped Lorentz-Mie particles. The following section describes the use of pulse shaping to control two-photon excitation in 3D trapped particles.

4.4 Control of multiphoton excitation in optically-trapped particles using phase-shaped ultrashort pulses

4.4.1 Experimental setup

For these experiments, the same trapping, position measurement, and dispersion compensation system was used as in Section 4.3. We used blue fluorescently-dyed 2.1μm polystyrene spheres (B0200 from Duke Scientific/Thermo Scientific), which absorb two-photon excitation from a wavelength range within our laser's SHG bandwidth (380-420nm). Back-reflected fluorescence signal, stretching from approximately 420-580nm, is divided between a camera and a spectrometer using a beamsplitter. The spectrometer consists of a Jobin-Yvon Triax 550 monochromator, coupled to a Jobin-Yvon Symphony Solo CCD camera for spectral capture capabilities. See Figure 3.3 for a diagram of the trapping microscope and spectrometer.

The white-light illumination wavelengths overlapped the fluorescence signal, so illumination had to be turned off whenever fluorescence was being collected. Photobleaching effects meant that fluorescence measurement had to start immediately after the particle was trapped. To achieve this, we diluted the sample, and located (but not trapped) individual particles with the aid of illumination. Once we had located a particle, we switched off the illumination and moved the sample so the particle was close enough to jump into the trap. The presence of the particle in the trap was verified by fluorescence signal visible on the CCD camera, and fluorescence spectral acquisition started within 1s.

The polymer particles were ablated and pushed along the beam at powers above 3.7mW; this ablation effect was worse for shorter pulse durations and higher powers. At powers above 15mW, the particles would be ejected axially from the trap almost immediately, and exhibited large shape deformations and craters. At powers between 3.7mW and 7mW, the particles could be trapped for

up to a few minutes (depending on the quality of laser alignment into the microscope system) until they were suddenly ejected axially from the trap. Imaging of these particles revealed that they had been drilled with narrow holes, an effect similar to that observed by Misawa and coworkers[10]. At powers between 1.8mW and 3mW, not far above the threshold where the 2.1μm particles could be trapped, the particles could be trapped for several minutes with no visible damage. In our experiments we used the lowest-power regime, with an average power of 3mW.

4.4.2 Results

In our first demonstration of shaped-pulse control of two-photon excitation in trapped particles, we controlled the total amount of two-photon excitation by stretching the pulse. As in Section 4.3.2, we first compensated for the dispersion already on the system, then used additional positive 2nd order dispersion to control pulse duration. For each pulse duration, we measured the fluorescence signal from a trapped particle over 5 seconds. To avoid photobleaching effects, we used a different particle for each measurement. For each pulse duration, we repeated the measurement with four different particles. The measured fluorescence spectra are shown in Figure 4.6. As expected, fluorescence intensity decreases as pulse duration increases. Note that because average power remained the same throughout the experiment, trap stiffness has remained invariant. In laser systems without a convenient method of rapidly switching between CW and mode-locked regimes, this method could be used to switch between a long pulse duration that avoids photobleaching and a short pulse duration that maximises fluorescence signal.

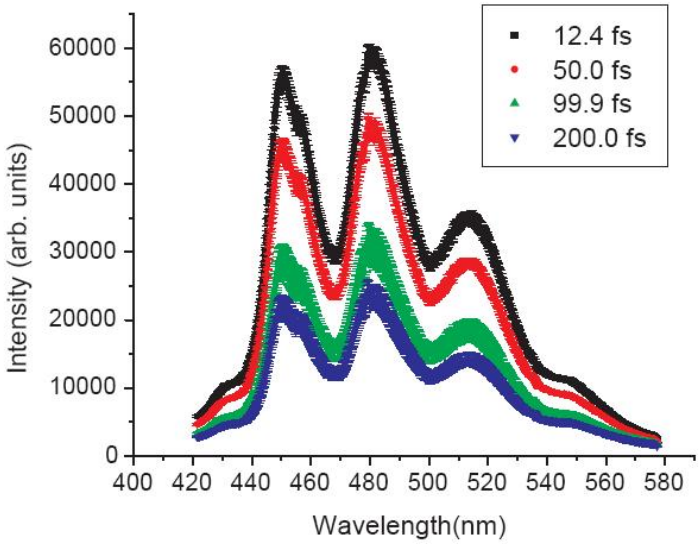

Figure 4.6:
Control of two-photon fluorescence in 3D trapped 2.1μm blue fluorescently-dyed polymer particles. Two-photon fluorescence spectra were measured under four different pulse durations, with pulse duration varied by introducing 2nd order dispersion with a pulse shaper. The same average power (3mW) was used for all measurements. Each curve is the average of four 5-second acquisitions with four different particles.

4.5 Selective multiphoton excitation in optical trapping

Section 4.4 above demonstrates just one possible method of multiphoton control in trapped particles. With other pulse shaping techniques, more advanced forms of control are possible. Some example applications include low-background single-beam coherent anti-Stokes Raman scattering (CARS) [22], highly accurate refractive index measurement [23], precise measurement of two-photon excitation spectra [25], and selective multiphoton excitation without wavelength tuning or filters [26].

We have performed preliminary investigations demonstrating two methods for selective two-photon excitation of trapped particles: amplitude shaping and phase-only shaping. These two methods are described below, along with their effects on the second harmonic spectra generated at the sample plane of our optical trapping system.

4.5.1 Amplitude shaping

The simplest method of controlling the two-photon absorption wavelength is by removing part of the laser's bandwidth. This can done by using the pulse shaper's amplitude shaping capabilities or, as in our case, by physically blocking part of the beam's bandwidth as it enters the pulse shaper. Blocking part of the beam results in the altered spectral shapes shown in Figure 4.7. The effect is to produce a choice of two fundamental spectra, each centred at a different wavelength and therefore producing SHG spectra centred at different wavelengths (See Figure 4.8).

The total amount of two-photon absorption at a given wavelength is proportional to the product of the laser's SHG spectral intensity at that wavelength and the molecule's two-photon absorption cross section, so we have in this way changed the wavelength of two-photon excitation.

The spectra in Figures 4.7 and 4.8 were measured at the trapping plane of our

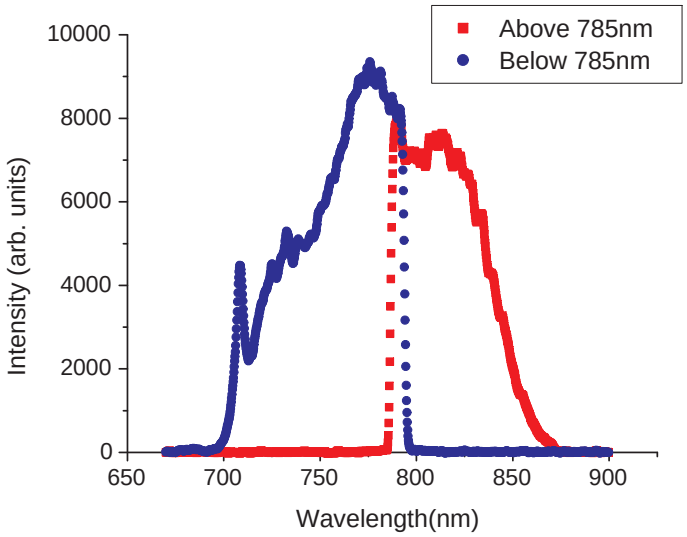

Figure 4.7:
Fundamental spectrum of the laser, as transmitted through the sample plane, showing the effects of amplitude modulation. This spectrum was scattered using a non-absorbing white card, and measured with the Ocean Optics USB 4000 spectrometer. The bandwidth of the laser was reduced by physically blocking part of the laser's spread spectrum as it entered the spatial light modulator (SLM) in the pulse shaper. The blue curve shows the result of blocking all intensity above 785nm, while the red curve was produced by blocking all intensity below 785nm.

microscope. We used dispersion-compensated pulses, produced by measuring and cancelling dispersion as in Section 3.4. Our original dispersion measurement can still be used to compensate the dispersion of these narrower-bandwidth spectra since the total phase delays seen by each wavelength as they travel through the system are independent of one another. Therefore, in our experiments each narrower-bandwidth spectrum is transform-limited (TL). For the SHG spectra in Figure 4.8, a thin BBO crystal was placed at the trapping plane.

4.5.2 Phase shaping

Although amplitude shaping can be used very effectively to confine multiphoton excitation to the higher- or lower- wavelength extremes of the SHG bandwidth,

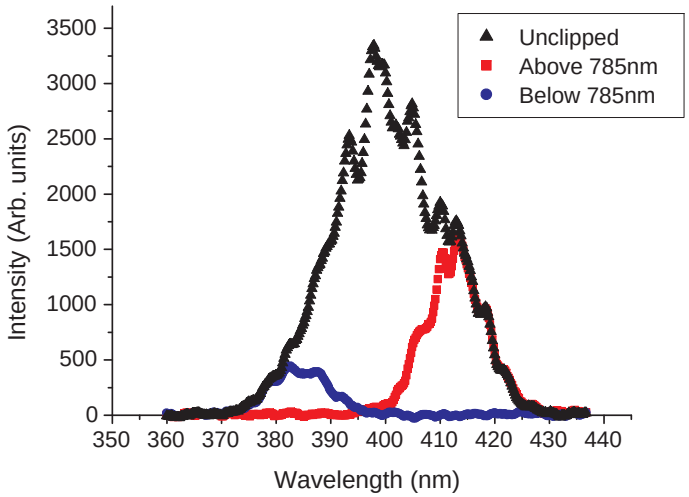

Figure 4.8:
Effect of amplitude shaping on the laser's SHG spectrum. The unclipped SHG spectrum (black) stretches from 370-425nm with a maximum at 395nm. Removing the laser's bandwidth below 785nm produces a SHG spectrum centred at 415nm (red), while removing the bandwidth above 785nm produces a SHG spectrum centred at 385nm (blue).

it is less effective at selectively exciting using narrow wavelength ranges within the SHG bandwidth. This is because as the fundamental laser bandwidth is restricted, the resulting SHG amplitude decreases quickly[76].

A second method of achieving wavelength selectivity is to use phase shaping alone. Through phase shaping it is possible to allow two-photon excitation within only a wavelength range as narrow as about 1nm wide, at nearly the amplitude afforded by TL pulses. The width and number of these allowed two-photon excitation ranges can be controlled as well[25]. The methods with the best excitation selectivity are based on binary phase functions, that is, phase functions that allow phase values of only 0 and π. For selective excitation of wider wavelength ranges, there are a number of additional options, including sinusoidal and 3rd order phase modulation.

In the following demonstration, SHG selectivity was achieved using 3rd order phase modulation. These phase functions are of the form $\phi(\omega) = \frac{1}{6}\gamma_3(\omega - \omega_0)^3$, where γ_3 is the amount of 3rd order dispersion in fs^3, and ω_0 is the centre frequency of the phase function. A peak is created in the SHG spectrum at $2\omega_0$, gradually sloping to lower background elsewhere. The magnitude of γ_3 determines how narrow the peak is; in theory the peak can be made arbitrarily narrow but this is limited in practise by the magnitude of the phase function that the pulse shaper's SLM can accurately reproduce.

We applied 3rd order phase functions to our dispersion-compensated pulses using the setup described in Section 3.4. Figure 4.9 shows the effect of 3rd order phase modulation on the laser's SHG spectrum, as measured in the trapping plane using a thin BBO crystal. "Shape 1" (blue circles) was created using $\gamma_3 = -8000fs^3$ and $\lambda_0 = 776$ nm, while "Shape 2" (red triangles) was created using $\gamma_3 = 8000fs^3$ and $\lambda_0 = 816$nm. The fundamental spectrum of our laser was left unchanged.

These phase functions localise SHG excitation less efficiently (that is, with more imperfect suppression of background excitation outside the wavelength range of interest) than amplitude shaping. However, this selectivity occurs

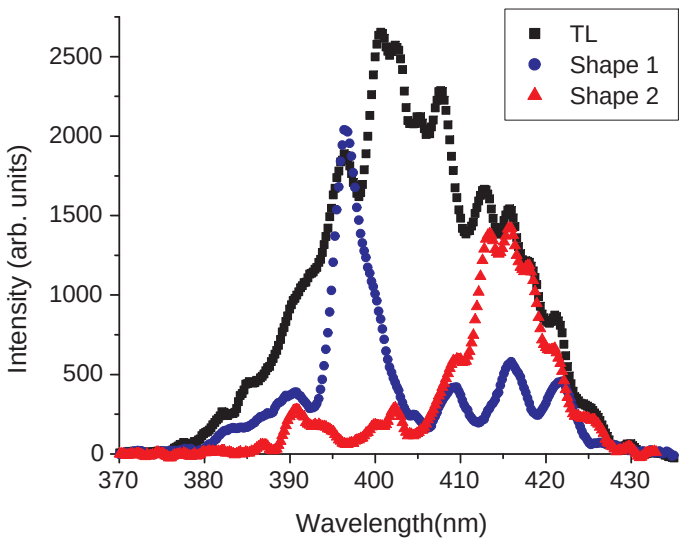

Figure 4.9:
Peaks created in the laser's SHG spectrum using 3rd order phase modulation, of the form $\phi(\omega) = \frac{1}{6}\gamma_3(\omega - \omega_0)^3$, where γ_3 is the amount of 2nd order dispersion in fs^3, and ω_0 is the centre frequency of the phase function, which determines the location of the SHG peak. The black curve shows the unshaped transform-limited (TL) spectrum. "Shape 1" (blue circles) was created using a phase function with $\gamma_3 = -8000 fs^3$, centred near the lower-wavelength end of the spectrum (776 nm), while "Shape 2" (red triangles) used $\gamma_3 = 8000 fs^3$, centred near the higher-wavelength end of the spectrum (816 nm).

without change to the shape or amplitude of the laser's fundamental spectrum, meaning that optical trapping is unaffected. Additionally, the excitation wavelength range of interest can be located anywhere within the SHG spectrum, rather than only the spectral edges, and multiple excitation wavelengths can be used simultaneously. Other phase function types should be able to offer significant decrease in background, leading to an improvement in selectivity[25, 26].

The phase shaping methods demonstrated above should allow future experiments to demonstrate selective two-photon excitation in trapped particles. This will require the use of spheres whose two-photon absorption spectra vary over the pulse's bandwidth, and which are not damaged by the ultrashort laser pulses. Reference [26] demonstrates selective two-photon excitation in a pair of dyed microspheres using a similar laser source to ours; in these experiments the microspheres were fixed in place rather than trapped.

4.6 Conclusion

4.6.1 Summary

These investigations show through theory and experiment (Lorentz-Mie regime) that optical trapping using pulsed lasers is independent of the pulse's duration or time profile. Material-dependent effects on optical trapping are outside the scope of our investigations, although they would be interesting subjects for future study. Optical trapping of silica and polymer particles was performed with transform-limited pulses of 12.9 femtosecond FWHM duration, by far the shortest pulse duration used in optical trapping to date. The pulse duration was systematically varied over 1.5 orders of magnitude using phase shaping, and observed to have no significant effects on optical trapping. As a result, it is possible to use phase shaping to control nonlinear processes in optically trapped particles without affecting optical trapping itself. This was demonstrated by using 2nd order phase functions to increase pulse duration, and observing the effects on two-photon fluorescence in trapped dyed polymer spheres. Two-photon

fluorescence decreased as pulse duration increased, as expected. Preliminary experiments on phase and amplitude shaping show the possibility of selective multiphoton excitation in trapped particles.

4.6.2 Reflections/Future work in optical trapping using short pulsed lasers

4.6.2.1 Pulsed laser trapping of Rayleigh-sized particles

The work described in this chapter indicates that trapping of Lorentz-Mie-sized particles is independent of pulse duration. A recent theoretical paper discussed the possibility of a material-independent pulse duration effect on optical trapping in the Rayleigh regime[71]. Our own theory and modelling indicate no pulse duration dependence in any size regime, but there have been no experiments addressing this question so far. Although we attempted to perform these measurements for Rayleigh-sized particles as well, the limited available trapping power (47mW at maximum) prevented us from trapping single 50nm or 100nm silica particles for long enough to make measurements. Gold, silver, and polymer have higher polarisability and therefore stronger trapping at the same average power, but nonlinear effects such as ablation and cavitation prevented us from trapping these materials with ultrashort pulses. Large polymer particles could be trapped without damage at low average powers, as described earlier in this thesis, but the average powers required for trapping Rayleigh-sized particles were far above this damage threshold.

An additional problem that limited our ability to study trapping of Rayleigh-sized particles was vibrational noise. The trapping system had to be elevated from the table to allow room for components such as the CCD camera and spectrometer, making the system more prone to vibrations. A custom-built solid metal sample stage, as well as the careful placement of vibration-dampening weights, greatly reduced vibrations. However, the remaining vibrations were significant enough that when single silica particles were briefly trapped, the

signal from these trapped particles was near the noise level of the system.

To solve these problems, future pulsed laser trapping experiments in the Rayleigh regime will need higher available power, for example, from an amplified system. Alternatively, a higher-power 100fs Ti:Sapphire source could be used, and stretched to different pulse durations using a prism pair, with resulting pulse duration estimated using autocorrelation. Although this method would not allow as fine a control of pulse profile and duration as reported in the experiments in this work, it could still indicate whether pulse duration has any effect at all. With a redesign of the pulse shaper to spread the 100fs pulse's approximately 9nm bandwidth over more SLM pixels, it would also be possible to use MIIPS and a pulse shaper to perform this experiment with high precision.

Trap stiffness and position detection could be enhanced by using particles with higher polarisability and scattering, provided these particles were not damaged by the pulsed laser. The sensitivity of position detection could be further enhanced by eliminating sources of electrical and vibrational noise.

4.6.2.2 Position detection via backscattered signal

Slight cavity shifts in the laser, as mentioned in Section 3.1, was a source of significant delay. These shifts changed output power by as much as 10% and changed cavity dispersion as well, rendering previous dispersion measurements inaccurate. When these shifts occurred, which was sometimes multiple times daily, the dispersion had to be remeasured so that dispersion compensation would be complete once more. To do this, the QPD position detecting setup had to be replaced by the SHG collection setup, and then reinstalled once dispersion was remeasured. This procedure typically took about 45 minutes, although with the arrival of a specially-designed SHG collection system from BioPhotonic Solutions in the last months of the project, this time was reduced to about 20 minutes. For the fluorescence studies, with no QPD system to remove or realign, checking the dispersion took only three minutes. The most accurate way to determine whether the laser cavity had shifted was by remeasuring the dis-

persion, since dispersion could sometimes change without a measurable power loss. Therefore, this procedure had to be repeated before and after each experiment, to ensure that dispersion had not changed. By cleaning the output coupler mount we managed to temporarily reduce the number of cavity shifts. Re-cleaning or replacing more cavity mounts may lead to further improvements. Another possible strategy is a redesign of the setup such that the QPD detects back-scattered rather than forward-scattered signal. Although this setup would be more difficult to align initially, it would allow the dispersion to be measured without removing the QPD each time.

4.6.2.3 Pulse precompression

The trapping microscope system is very dispersive compared to many optical systems, and to compensate this dispersion requires a phase function that is at the very limit of what the pulse shaper can accurately apply. Large phase functions require large amounts of phase function wrapping, a pulse shaper limitation described in Section 2.2.3. Once wrapping becomes too large for the shaper to handle (maximum wrap density is somewhere around 1 wrap / 5 pixels), the pulse shaper can no longer reliably reproduce the desired phase function, leading to phase inaccuracies, and to unintentional amplitude modulation. We built a ZF4 prism pair to pre-compensate for some dispersion, using the methods described in Section 2.2.1, but found that the prism pair exacerbated the system's spatial chirp problems. As a compromise, we instead introduced negative GVD by translating the pulse shaper's grating, compensating for some dispersion without increasing system complexity or introducing additional spatial chirp. Even with this partial precompensation, we had to take care not to introduce phase functions that would combine with the large remaining dispersion compensation function to cause significant wrapping-induced inconsistencies. Through a more accurately designed precompressor, it would be possible to precompensate for virtually all dispersion without introducing spatial chirp. This would allow a greater range of phase functions to be used in future experiments.

4.6.2.4 Separate probe and trapping beams

For future work, it may be useful to employ ultrashort pulsed lasers as probe beams only, rather than as combination probe and trapping beams. At the average powers required for strong optical trapping, the high peak powers of ultrashort pulsed lasers will damage many materials and will quickly photobleach many fluorescent dyes. Although <50fs lasers offer decreased photobleaching in two-photon fluorescence, this is because they allow extremely low average powers to be used[21], so their advantages are not realised at typical optical trapping powers. Additionally, current ultrashort lasers are not as stable as CW lasers, and pulse shapers cause slight amplitude and spatial profile changes in the beam when switching between two very different phase functions[39]. These properties make ultrashort pulsed lasers less suitable as trapping beams in applications requiring high stability. However, as probe beams, ultrashort pulsed lasers offer extremely high efficiency and with the added flexibility of phase/amplitude shaping, can enable unique nonlinear studies in optically trapped particles.

Chapter 5

Bessel beam compensation

5.1 Introduction

Bessel beams are solutions to the Helmholtz equation that are propagation-invariant[14]. Zero-order Bessel beams, the most commonly-used variety, have spatial intensity profiles that are two-dimensional zeroth-order Bessel functions of the first kind. Unlike plane waves, which are also diffraction-free solutions of the wave equation, these Bessel beams have narrow central spots, whose radii can be comparable to the wavelength of light. The resulting beam has a small central maximum that propagates without spreading, creating a needle-like shape. In addition to their long propagation distance, Bessel beams that are partially obstructed can self-reconstruct after propagating for some distance[15]. Due to these properties, Bessel beams have applications in areas such as long-distance guiding, machining, studies of high-intensity phenomena, and cellular transfection.

True Bessel beams contain infinite energy and are not physically realisable, so the Bessel beams used in practise are Bessel-like beams, true Bessel beams multiplied by some intensity envelope. These experimentally realisable beams do not propagate indefinitely without spreading, but can propagate for several times the Rayleigh range while maintaining a radius constant within a factor of

1/e[14].

A number of methods exist for generating experimental Bessel beams. The original experimental Bessel beam demonstration by Durnin and coworkers used a circular slit in combination with a lens[14]. A popular current method is the use of an axicon, also known as a conical lens. The axicon has the advantage of high efficiency (as in a standard lens), and can be used as a standalone lens, or etched into the tip of an optical fibre[77]. Another useful way to generate Bessel beams is using a spatial light modulator in combination with an axicon; in this way, multiple Bessel beams can be generated simultaneously and steered independently in 3D[78].

Bessel beams can be generated from both CW and pulsed laser sources. Ultrashort Bessel beams are of great interest in studies of high-intensity phenomena, including high-harmonic generation[79], self-focusing, filamentation, and 3D solitons. Lower-intensity ultrashort Bessel beams are attractive for applications in micromachining. They have been used in transfection through photoporation, the process of creating transient holes in cellular membranes through which membrane-impermeable substances such as drugs or DNA can be introduced[80]. The efficiency of photoporation with Gaussian beams depends highly on the focal location with respect to the cell surface, but this focal distance is difficult to determine. The focal area of a Bessel beam is very long, so Bessel beams offer high-efficiency photoporation without the need to accurately determine focal distance[80]. In non-biological machining, Amako and co-workers used 100-500fs Bessel beams to drill long thin holes in glass; they noticed that longer pulses tended to produce larger holes[81]. In another machining work, Matsuoka and co-workers used pulsed nanosecond Bessel beams to drill holes in metal, and found that the holes had less taper than those drilled using Gaussian beams[82].

This chapter describes the use of MIIPS for measuring and compensating the dispersion of a microscope system that uses an axicon to generate a Bessel-like beam. This system is currently being used in ongoing work on ultrashort Bessel

beam photoporation. The origins of this project are an idea from my original fellowship proposal in November 2006. I had proposed to perform photoporation using dispersion-compensated 12fs pulses rather than the uncompensated 100fs pulses typically used, hypothesising that the shorter pulse durations would allow the use of lower average powers. Photoporation is a multiphoton process, while the accompanying thermal damage is a single-photon process, so lower average powers should produce cleaner membrane holes and therefore increase cellular survival. A June 2008 paper by Uchugonova and co-workers, in which sub-20fs pulses were used for photoporation with very low average powers, indicates the feasibility of these ideas [20].

Similar enhancement could be expected in non-biological machining applications. Many studies of high-intensity phenomena use Bessel beams with durations as low as about 10fs; however, to minimise temporal dispersion, these studies use only reflective optics to guide and focus the beam[83], and/or generate the Bessel beam using thin-film, holographic, or fibre methods. These methods of achieving Bessel beams do not lend themselves to flexibility or integration with existing highly-dispersive microscope systems, and to the best of our knowledge, ultrashort Bessel beams have not been applied to photoporation or machining.

In addition to its application in photoporation, this system has the ability to modify the temporal and spectral profile of the Bessel beam, thanks to the pulse shaper. This will make it possible to study the effects of pulse shaping on the spatial profile of the axicon-created Bessel beam. The dispersion compensation reported in this chapter overcomes the major obstacle of unknown temporal dispersion, and clears the way toward studies of Bessel beams with custom spectral and temporal shape.

5.2 Experimental setup

For our studies using Bessel beams, we built an upright axicon system, with the beam incident on the sample plane from above. The axicon system used the same 12fs 780nm, 80MHz laser source and pulse shaper as the optical trapping system, as described in Chapter 3. A diagram of the axicon system is shown in Figure 5.1, and a photograph is shown in Figure 5.2. In the configuration shown, the microscope is set up for SHG detection, for use in the MIIPS dispersion measurement and compensation algorithm. The Microscope Detection Unit (MDU) provided along with the pulse shaper from BioPhotonic Solutions, Inc. was designed only for use in inverted microscopes, so we used our own second harmonic (SHG) generation/collection design to couple SHG signal from the sample plane into an Ocean Optics USB 4000 fibre spectrometer (Figure 5.1). This SHG collection design is described in Section 3.4. Although the setup shown in Figure 5.1 does not include illumination or a camera for imaging, these can easily be incorporated, for example, by replacing the mirror just before the axicon with a dichroic mirror to allow illumination to enter from the top, and replacing the fibre and filter with a CCD camera after dispersion has been measured. We use a CCD camera in this manner to image the Bessel beam as reported below, although no illumination is incorporated in this case.

5.3 Results

To verify that our axicon system successfully produced a Bessel beam, we imaged the beam onto a CCD camera placed after the axicon. Due to the limited resolution of the CCD sensor, we first had to expand the beam using a demagnifying telescope, which we placed directly after the axicon. The beam then was imaged by the CCD camera. Figure 5.3 shows the resulting images of the beam, with the camera placed at the beam's narrowest point (b) and at a 2.86 mm axial distance from the beam's narrowest point (a). The beam had a narrow focal spot over this entire range; the images here were overexposed

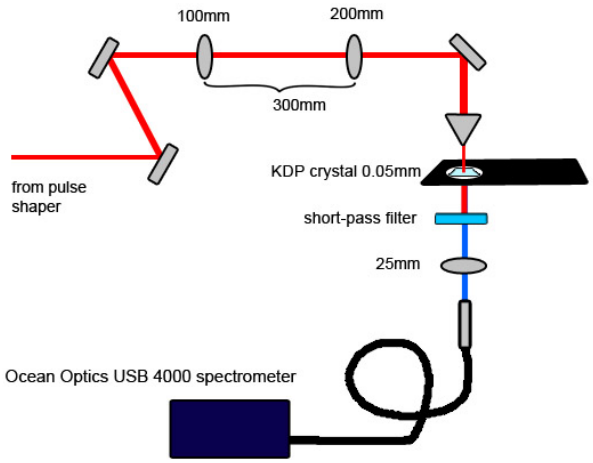

Figure 5.1:
The axicon system, set up for collection of second harmonic generation (SHG) from the sample plane. Upon entering the microscope through a periscope, the beam is magnified and passes through a 5^o axicon. The Bessel-like beam formed by the axicon passed through a 0.05mm thick KDP crystal (cut for phase matching at 800nm) at the sample plane, generating SHG signal. A UV-grade fused silica lens collects the SHG signal and focuses it onto an Ocean Optics USB4000 fibre spectrometer. A short-pass filter prevents the laser light from saturating the spectrometer.

to show the structure in the rings of the Bessel beam pattern. The intensity patterns visible in Figure 5.3 (a) and (b) consist of concentric rings of decreasing intensity, as expected for a Bessel beam. In Figure 5.3 a) there is also a dark band of missing rings in our observed intensity pattern, which may be due to beat-like destructive interference between the discrete frequencies that make up our broad modelocked pulses. This phenomenon is the subject of ongoing experimental investigations.

We were able to successfully compensate for dispersion in the axicon system, for the 5-degree axicon shown in Figure 5.1 as well as for microscope objectives. Dispersion compensation resulted in near-transform-limited pulses with a (actual duration)/(transform-limited duration) ratio of 1.01, reflecting virtually no remaining phase distortion. The measured dispersion of our axicon system, including the 5-degree axicon, is shown in Figure 5.4. This system introduces much less dispersion than the optical trapping system (see Figure 3.8), because

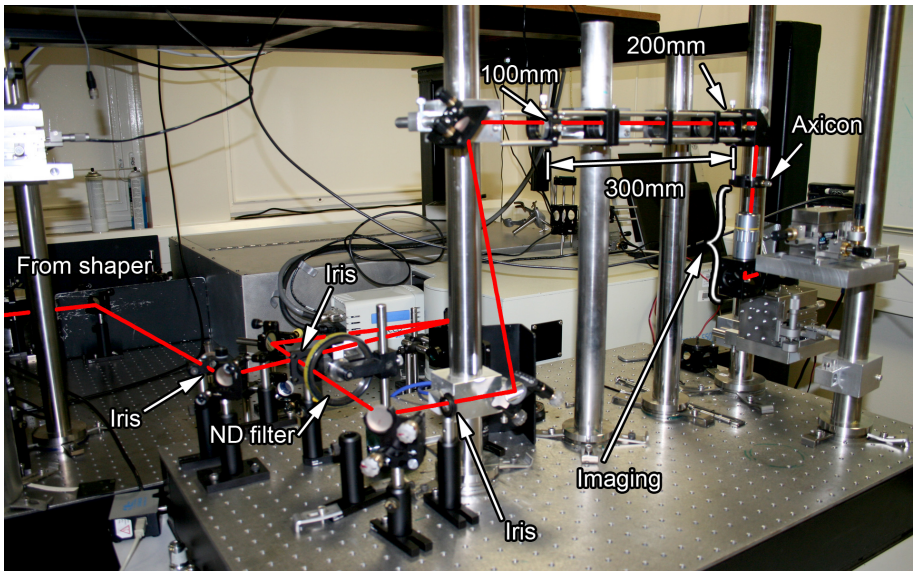

Figure 5.2:
Photograph showing the axicon system, with the beam path traced for clarity. From the pulse shaper output, the beam is sent to the axicon system optical table. The beam passes through a series of irises, with folding mirrors to increase the path length between irises. These irises allow alignment to be adjusted for slight changes in the relative heights of the floated main optical table and the non-floated axicon table. The beam passes through an ND filter wheel, used to attenuate intensity if necessary. After a periscope, the beam is expanded and enters the 5-degree axicon from above. In the photograph, the SHG detection system has been removed and replaced with the imaging system that produced the Bessel beam images shown in Figure 5.3.

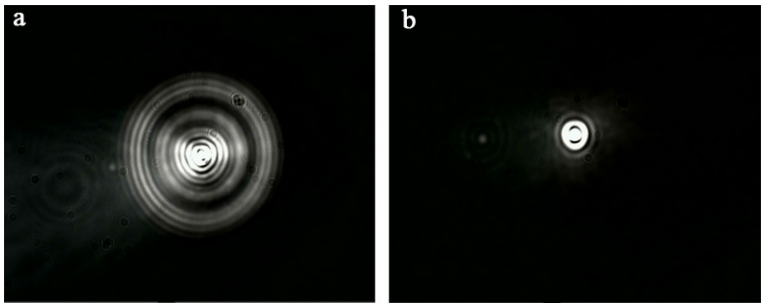

Figure 5.3:
Images of the Bessel beam created by a 5^o axicon in the upright microscope system, with dispersion compensated at the output of the axicon (FWHM duration: 12.8 fs). A demagnifying telescope then expanded the beam which was then imaged by a CCD camera. Image a) shows the Bessel beam imaged with the camera translated an axial distance of 2.86 mm from the beam's narrowest point. Image b) shows the Bessel beam imaged at its narrowest point. Both images have been overexposed to show structure in the beam pattern's outer rings. The faint secondary patterns are backreflections, and not part of the beam profile.

it contains an axicon rather than a highly-dispersive high-NA microscope objective. Most of the second-order dispersion introduced by the telescopes in the optical system has been pre-compensated by the placement of the grating within the pulse shaper (see Section 3.4.2), so second-order dispersion no longer dominates the dispersion function, as in Figure 3.8. Now it is possible to see the contributions of third-order and higher-order dispersion, introduced by lens anti-reflection coatings, dielectric mirror coatings, the laser cavity, the pulse shaper, and to a small degree by BK7 glass.

5.4 Conclusion

5.4.1 Summary

In our experiments so far, we have constructed an upright axicon system for use in future photoporation work. The system incorporates an axicon instead of a microscope objective, and a 12fs pulsed Ti:sapphire laser. The optical system also contains a pulse shaper, which is used to implement the MIIPS dispersion compensation method with the aid of feedback signal from a KDP

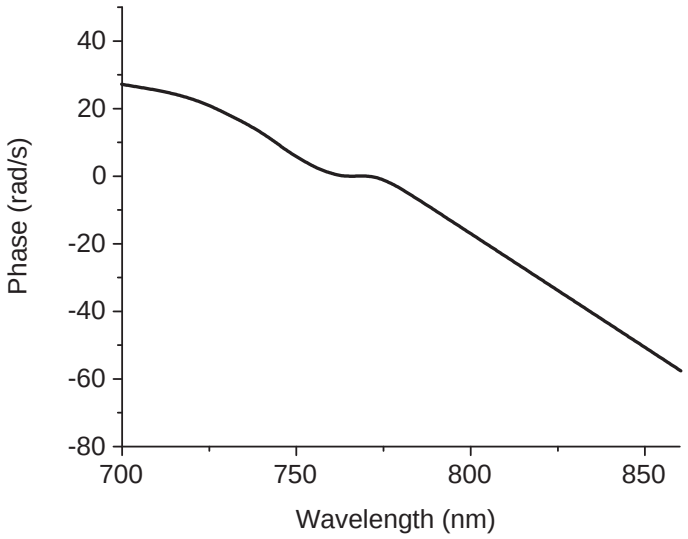

Figure 5.4:
Measured dispersion of the entire axicon system, including laser and shaper. Note that this system introduces much less dispersion than the optical trapping system (Figure 3.8), because it contains an axicon rather than a high NA microscope objective.

crystal placed at the sample plane. We were able to successfully compensate for all orders of dispersion, resulting in near-transform-limited pulses at the sample plane. Future experiments will use this system to transfect cells, and to investigate the effects of pulse temporal shape on the spatial profile of the resulting Bessel beam.

5.4.2 Reflection and future outlook

The first stages of the project focused on Gaussian beam photoporation, using microscope objectives for focusing. We tried a variety of microscope objectives with different working distances and numerical apertures. Each new microscope objective required a telescope change and system realignment, to overfill the various back aperture diameters, as well as characterisation of the spot size and beam power at the sample. In addition, the dispersion had to be measured separately for each microscope objective. The more dispersive microscope objectives were the hardest for the MIIPS algorithm to measure, so the first dispersion measurement for some microscope objectives would take hours to complete. However, after this first measurement, subsequent shifts in laser cavity dispersion or system changes (e.g. changing the telescope) caused comparatively small changes in total system dispersion, and refinement of the original dispersion measurement only took a couple of minutes. The axicon introduced a very small amount of dispersion compared to the microscope objectives, so once we shifted our focus to an axicon system, dispersion measurement was much easier.

Other experimental challenges were imposed by the limited space available for the setup. The floated optical table already contained the optical trapping system, so we had to construct the axicon system and its microscope on an auxiliary nonfloated table. Although the experiments were not sensitive to the increase in vibration compared to the floated table, the constant slight drift in the height of the floated table necessitated careful construction of the system so that it could be realigned frequently to compensate for this drift. The use

of pairs of irises and mirrors (see diagram in Figure 3.3) minimised the impact of realignment on the microscope system, but the increased path length meant that realignment was a daily occurrence.

A primary source of difficulty we have faced in our preliminary experiments on photoporation is inherent to work with cultured cells. Many factors affect the efficiency of photoporation, including exposure time, power, number of exposures, and spot size. A systematic study of all of these factors would take prohibitively long, due to the time required to culture cells, the time required to photoporate individual cells, and the natural variation between batches of cultured cells and individual cells within a single batch. Although previous work in femtosecond photoporation reported the parameters they found to be optimum, their pulse durations were on the order of 100-200 fs, so their peak powers were orders of magnitude lower than those of our 12 fs pulses at the same average powers[19]. Consequently we found that their parameters produced very poor results for our system, and we spent some weeks exploring the parameter space for our own system. Eventually the focus of our experiments changed from Gaussian beam photoporation to Bessel beam photoporation, which will necessitate further parameter space exploration as these experiments continue.

Another question that will need to be addressed as these experiments continue is whether dispersion remains constant along the axicon-created Bessel beam's propagation distance. The Bessel beam profile is formed from overlapping conical wavefronts, each of which originates from a different point along the radius of the axicon. The axicon's thickness, and therefore dispersion, decreases radially, so the amount of dispersion may vary along the Bessel beam's propagation distance. If so, then a dispersion measurement for an axicon-created Bessel beam is only valid for one particular plane, and the pulse's time profile will be stretched and distorted in other planes, impacting the efficiency of machining or photoporation in these other planes. To eliminate this effect, the Bessel beam could be fabricated using a method for which dispersion is constant, such as thin-film methods, if these could be adapted for use in a microscope.

Future experiments may also look at the effect of pulse temporal profile on the Bessel beam's spatial appearance. It is expected that as pulse duration decreases, the Bessel beam's outer rings will become less intense compared to the central maximum, as observed by Grunwald and coworkers[84]. As we use pulse shaping to change the time profile of ultrashort pulses, the fringe intensities are expected to change as well. A coworker Michael Mazilu has suggested that the relative intensities of the fringes may directly indicate the pulse's temporal profile. In this case, the use of a dispersion-free Bessel beam generation method (such as thin-film Bessel beam generation) would provide simple single-beam autocorrelation measurements of the ultrashort pulse temporal profile wherever the element is placed. Additional theory and experiment are needed to see whether this is indeed the case, and if so, whether the resolution provided (due to the absence of signal between the discrete rings) will be useful. Any experiments along these lines will have to take the spatial profile of the Gaussian ultrashort pulse into account. Although ideally the beam should have a Gaussian spatial profile that is invariant as the spectral phase is modified, experimentally we have found slight spatial changes, especially as the pulse shaper changes between very different phase functions. In the trapping experiments, these spatial changes had relatively small effects, but the effects are noticeable in the lower-intensity fringes of the beam profile, and may pose a challenge in these experiments.

Chapter 6

Conclusions

The year of work described in this thesis represents the first combination of the fields of optical trapping, pulse shaping, and Bessel beam photoporation. Dispersion-compensated and phase-shaped ultrashort pulses were used in optical trapping for the first time, and for preliminary studies in Bessel beam photoporation.

The thesis began with a description of the motivations for using ultrashort pulses in nonlinear excitation, with high peak power leading to high efficiency, and large bandwidth leading to pulse shaping possibilities. The problem of temporal dispersion was discussed, and a number of strategies for measuring and eliminating temporal dispersion were reviewed.

The following chapter began by describing the construction of an optical trapping system with position detection, and its interfacing with a spectrometer. The next section describes how a pulse shaper implementing the Multiphoton Intrapulse Interference Phase Scan (MIIPS) method of dispersion measurement and compensation was installed and adapted for use with the high-NA microscope objectives used in our home-built trapping microscope. Ultimately we were able to achieve dispersion-compensated 12-13fs pulses at the trapping plane (with exact duration depending on day-to-day variation in the laser's spectral profile), with the capability of more complex phase and amplitude shaping.

We used these dispersion-compensated pulses along with a QPD position detection system to study the effects of pulse duration on the 3D trapping of 780nm silica particles. We found, in agreement with our theory, that optical trap stiffness depends on average power, not on the laser's time profile. That is, for high-repetition-rate pulsed lasers, pulse duration has no material-independent effect on optical trapping.

Once we had determined that there would be no effect on the trapping process, we were able to use phase shaping to control two-photon excitation in 3D trapped 1.9μm blue fluorescently-dyed polymer. We also demonstrated a pulse shaping technique that allows wavelength-selective multiphoton excitation: by applying a third-order phase function to dispersion-compensated ultrashort pulses, we confined two-photon excitation to higher or lower wavelengths within the pulse's 2nd order spectrum, without changing the laser's fundamental spectrum. We showed similar selective two-photon excitation by blocking part of the laser's spectrum in the shaper, restricting the fundamental spectrum to higher- or lower- wavelength regions. This method produced better selectivity but required changing the laser's fundamental spectrum and therefore its trapping characteristics. These demonstrations open the door to the use of other pulse shaping techniques for further control and characterisation of trapped particles.

This thesis also describes the initial steps in an ongoing Bessel beam photoporation project, including construction of a microscope for photoporation and the successful measurement and compensation of dispersion in this microscope. As opposed to earlier methods of generating ultrashort Bessel beams, this system can easily be incorporated into microscope systems, and is able to accommodate additions of filters, shutters, telescopes, etc to the beam path. Future studies with this system will perform cellular transfection, and investigate the effects of pulse temporal profile on the spatial characteristics of the Bessel beam.

Acknowledgements

This thesis would not have been possible without the help, support, and encouragement of the many wonderful people I met during my year in St Andrews.

I would like to begin by thanking Steve Lee for all his help in setting up the QPD position detection and data acquisition program, as well as the illumination for the optical trapping microscope. I am grateful for all his advice on the optical trapping experiments, and for all his support and encouragement over the year.

Michael Mazilu has been a wonderful resource, providing the Lorentzian curve fitting program, as well as the outline for the theory in Section 4.2. Michael also helped tremendously with experimental troubleshooting, and many discussions of theory and experimental design, as well as many words of wisdom about life as a postgraduate student.

I was fortunate to work closely with Xanthi Tsampoula on the Bessel beam / photoporation project. I'm grateful to Xanthi for giving me a valuable introduction to the world of photoporation and Bessel beams, and for culturing, porating, and analysing the cells used in our photoporation studies. Xanthi also designed the home-built microscope we used in these experiments, and both designed and implemented the adaptation of this microscope to use an axicon. I'm pleased to know that Xanthi is continuing this work, and supervising transition to another graduate student as the project continues into its next stages.

Iain Cormack helped me tremendously in my first weeks at St Andrews, giving me a first introduction to aligning and building optical systems, so valuable

from someone fresh out of the world of simulation and theory.

Chris Leburn and Tom Brown were lifesavers on more than one occasion. They taught me a ton about how to align and troubleshoot the femtosecond laser, and stepped in to save the day when I couldn't get the laser mode-locked, or when it had to be moved to another lab.

I am grateful to Phillip Jess, now also a new Californian, for designing the majority of the optical trapping microscope, and for valuable guidance on how to install the monochromator and align the system.

Igor Pastirk has been a wonderful collaborator, giving me patient over-the-phone technical support for installing and troubleshooting the MIIPS pulse shaper.

It has been a pleasure working with Kishan Dholakia as my adviser - he has been a wonderful coordinator of resources, and I couldn't ask for a more supportive adviser.

Finally, I would like to say a huge thank-you to all the people in the Physics department who have helped and welcomed me in a myriad of ways over the year, whether through lending their technical expertise, providing support and encouragement, or hanging out during coffee, lunches, pub trips, photography outings, and hillwalking . You have all made it a great year, and I will miss you tons.

Bibliography

[1] A. Ashkin, J. Dziedzic, J. Bjorkholm, and S. Chu, "Observation of a single-beam gradient force optical trap for dielectric particles," *Optics Letters* **11**(5), pp. 288–290, 1986.

[2] P. Van der Straten and H. J. Metcalf, *Laser cooling and trapping*, Springer, 1999.

[3] K. Svoboda, C. Schmidt, B. Schnapp, and S. Block, "Direct observation of kinesin stepping by optical trapping interferometry," *Nature* **365**(6448), pp. 721–727, 1993.

[4] L. Ghislain and W. Webb, "Scanning-force microscope based on an optical trap," *Optics Letters* **18**, pp. 1678–1678, 1993.

[5] J. Curtis, B. Koss, and D. Grier, "Dynamic holographic optical tweezers," *Optics Communications* **207**(1-6), pp. 169–175, 2002.

[6] K. König, "Laser tweezers are sources of two-photon excitation," *Cellular and Molecular Biology (Noisy-le-grand, France)* **44**, pp. 721–733, Jul 1998.

[7] B. Agate, C. T. A. Brown, W. Sibbett, and K. Dholakia, "Femtosecond optical tweezers for in-situ control of two-photon fluorescence," *Optics Express* **12**(13), pp. 3011–3017, 2004.

[8] L. Malmqvist and H. M. Hertz, "2nd-harmonic generation in optically trapped nonlinear particles with pulsed lasers," *Applied Optics* **34**(18), pp. 3392–3397, 1995.

[9] E. V. Perevedentseva, A. V. Karmenyan, F. J. Kao, and A. Chiou, "Second harmonic generation of biotin and biotin ester microcrystals trapped in optical tweezers with a mode-locked Ti : Sapphire laser," *Scanning* **26**, pp. I78–I82, Sept. 2004.

[10] H. Misawa, M. Koshioka, K. Sasaki, N. Kitamura, and H. Masuhara, "Three-dimensional optical trapping and laser ablation of a single polymer latex particle in water," *Journal of Applied Physics* **70**, p. 3829, 1991.

[11] J. W. Chan, H. Winhold, S. M. Lane, and T. Huser, "Optical trapping and coherent anti-Stokes Raman scattering (CARS) spectroscopy of submicron-size particles," *IEEE Journal of Selected Topics in Quantum Electronics* **11**(4), pp. 858–863, 2005.

[12] A. Fontes, K. Ajito, A. A. R. Neves, W. L. Moreira, A. A. de Thomaz, L. C. Barbosa, A. M. de Paula, and C. L. Cesar, "Raman, hyper-Raman, hyper-Rayleigh, two-photon luminescence and morphology-dependent resonance modes in a single optical tweezers system," *Physical Review E* **72**(1), 2005.

[13] D. Morrish, X. S. Gan, and M. Gu, "Scanning particle trapped optical microscopy based on two-photon-induced morphology-dependent resonance in a trapped microsphere," *Applied Physics Letters* **88**(14), 2006.

[14] J. Durnin, J. J. Miceli, and J. H. Eberly, "Diffraction-free beams," *Physical Review Letters* **58**, pp. 1499–1501, Apr 1987.

[15] S. R. Mishra, "A vector wave analysis of a Bessel beam," *Optics Communications* **85**, pp. 159–161, Sept. 1991.

[16] L. Schermelleh, S. Thalhammer, W. Heckl, H. Pösl, T. Cremer, K. Schütze, and M. Cremer, "Laser microdissection and laser pressure catapulting for the generation of chromosome-specific paint probes," *Biotechniques* **27**, pp. 362–367, Aug 1999.

[17] M. Tsukakoshi, S. Kurata, Y. Nomiya, Y. Ikawa, and T. Kasuya, "A novel method of DNA transfection by laser microbeam cell surgery," *Applied Physics B: Lasers and Optics* **35**, pp. 135–140, Nov. 1984.

[18] A. Vogel and V. Venugopalan, "Mechanisms of pulsed laser ablation of biological tissues," *Chemical Reviews* **103**(2), pp. 577–644, 2003.

[19] D. Stevenson, B. Agate, X. Tsampoula, P. Fischer, C. T. A. Brown, W. Sibbett, A. Riches, F. Gunn-Moore, and K. Dholakia, "Femtosecond optical transfection of cells: viability and efficiency," *Optics Express* **14**(16), pp. 7125–7133, 2006.

[20] A. Uchugonova, K. König, R. Bueckle, A. Isemann, and G. Tempea, "Targeted transfection of stem cells with sub-20 femtosecond laser pulses," *Optics Express* **16**(13), pp. 9357–9364, 2008.

[21] P. Xi, Y. Andegeko, L. R. Weisel, V. V. Lozovoy, and M. Dantus, "Greater signal, increased depth, and less photobleaching in two-photon microscopy with 10 fs pulses," *Optics Communications* **281**(7), pp. 1841–1849, 2008.

[22] N. Dudovich, D. Oron, and Y. Silberberg, "Single-pulse coherently controlled nonlinear Raman spectroscopy and microscopy," *Nature* **418**(6897), pp. 512–514, 2002.

[23] Y. Coello, B. Xu, T. Miller, V. Lozovoy, and M. Dantus, "Group-velocity dispersion measurements of water, seawater, and ocular components using Multiphoton Intrapulse Interference Phase Scan," *Applied Optics* **46**(35), pp. 8394–8401, 2007.

[24] B. Xu, J. M. Gunn, J. M. D. Cruz, V. V. Lozovoy, and M. Dantus, "Quantitative investigation of the Multiphoton Intrapulse Interference Phase Scan method for simultaneous phase measurement and compensation of femtosecond laser pulses," *Journal of the Optical Society of America B* **23**(4), pp. 750–759, 2006.

[25] V. Lozovoy, B. Xu, J. Shane, and M. Dantus, "Selective nonlinear optical excitation with pulses shaped by pseudorandom Galois fields," *Physical Review A* **74**(4), p. 41805, 2006.

[26] J. Dela Cruz, I. Pastirk, M. Comstock, V. Lozovoy, and M. Dantus, "Use of coherent control methods through scattering biological tissue to achieve functional imaging," *Proceedings of the National Academy of Sciences, USA* **101**(49), pp. 16996–7001, 2004.

[27] J. B. Guild, C. Xu, and W. W. Webb, "Measurement of group delay dispersion of high numerical aperture objective lenses using two-photon excited fluorescence," *Journal of Applied Optics* **36**(1), pp. 397–401, 1997.

[28] M. S. Demokan, *Mode-Locking in Solid-State and Semiconductor Lasers*, John Wiley & Sons Ltd., 1982.

[29] BK7 refractive index data from Schott Optical Glass Catalog, Schott Glass Technologies Inc. (1992).

[30] F. Salin and A. Brun, "Dispersion compensation for femtosecond pulses using high-index prisms," *Journal of Applied Physics* **61**(10), pp. 4736–4739, 1987.

[31] R. L. Fork and O. E. Martinez, "Negative dispersion using pairs of prisms," *Optics Letters* **9**(5), p. 150, 1984.

[32] E. Treacy, "Optical pulse compression with diffraction gratings," *IEEE Journal of Quantum Electronics* **5**(9), pp. 454–458, 1969.

[33] S. Akturk, X. Gu, M. Kimmel, and R. Trebino, "Extremely simple single-prism ultrashort-pulse compressor," *Optics Express* **14**(21), pp. 10101–10108, 2006.

[34] R. Szipocs, K. Ferencz, C. Spielmann, and F. Krausz, "Chirped multilayer coatings for broadband dispersion control in femtosecond lasers," *Optics Letters* **19**(3), p. 201, 1994.

[35] F. X. Kaertner, U. Morgner, R. Ell, T. Schibli, J. G. Fujimoto, E. P. Ippen, V. Scheuer, G. Angelow, and T. Tschudi, "Ultrabroadband double-chirped mirror pairs for generation of octave spectra," *Journal of the Optical Society of America B* **18**(6), pp. 882–885, 2001.

[36] R. Paschotta, G. J. Spuhler, D. H. Sutter, N. Matuschek, U. Keller, M. Moser, R. Hovel, V. Scheuer, G. Angelow, and T. Tschudi, "Double-chirped semiconductor mirror for dispersion compensation in femtosecond lasers," *Applied Physics Letters* **75**(15), pp. 2166–2168, 1999.

[37] J. Jasapara and W. Rudolph, "Characterization of sub-10-fs pulse focusing with high-numerical-aperture microscope objectives," *Optics Letters* **24**(11), pp. 777–779, 1999.

[38] A. M. Weiner, "Femtosecond pulse shaping using spatial light modulators," *Review of Scientific Instruments* **71**(5), pp. 1929–1960, 2000.

[39] M. Wefers and K. Nelson, "Analysis of programmable ultrashort waveform generation using liquid-crystal spatial light modulators," *Journal of the Optical Society of America B* **12**, pp. 1343–1343, 1995.

[40] R. Trebino, K. W. DeLong, D. N. Fittinghoff, J. N. Sweetser, M. A. Krumbugel, B. A. Richman, and D. J. Kane, "Measuring ultrashort laser pulses in the time-frequency domain using frequency-resolved optical gating," *Review of Scientific Instruments* **68**(9), pp. 3277–3295, 1997.

[41] I. Amat-Roldán, I. Cormack, P. Loza-Alvarez, E. Gualda, and D. Artigas, "Ultrashort pulse characterisation with SHG collinear-FROG," *Optics Express* **12**(6), pp. 1169–1178, 2004.

[42] D. N. Fittinghoff, J. A. Squier, C. P. J. Barty, J. N. Sweetser, R. Trebino, and M. Mueller, "Collinear type II second-harmonic-generation frequency-resolved optical gating for use with high-numerical-aperture objectives," *Optics Letters* **23**(13), pp. 1046–1048, 1998.

[43] I. Amat-Roldán, I. G. Cormack, P. Loza-Alvarez, and D. Artigas, "Starch-based second-harmonic-generated collinear frequency-resolved optical gating pulse characterization at the focal plane of a high-numerical-aperture lens," *Optics Letters* **29**(19), pp. 2282–2284, 2004.

[44] C. C. Chang, H. P. Sardesai, and A. M. Weiner, "Dispersion-free fiber transmission for femtosecond pulses by use of a dispersion-compensating fiber and a programmable pulse shaper," *Optics Letters* **23**(4), pp. 283–285, 1998.

[45] V. V. Lozovoy, I. Pastirk, and M. Dantus, "Multiphoton Intrapulse Interference. IV. Ultrashort laser pulse spectral phase characterization and compensation," *Optics Letters* **29**(7), pp. 775–777, 2004.

[46] M. Dantus, V. V. Lozovoy, and I. Pastirk, "MIIPS characterizes and corrects femtosecond pulses," *Laser Focus World* **43**, pp. 101–104, 2007.

[47] V. V. Lozovoy, I. Pastirk, K. A. Walowicz, and M. Dantus, "Multiphoton intrapulse interference. ii. control of two- and three-photon laser induced fluorescence with shaped pulses," *The Journal of Chemical Physics* **118**(7), pp. 3187–3196, 2003.

[48] V. V. Lozovoy, B. Xu, Y. Coello, and M. Dantus, "Direct measurement of spectral phase for ultrashort laser pulses," *Opt. Express* **16**(2), pp. 592–597, 2008.

[49] B. von Vacano, T. Buckup, and M. Motzkus, "Shaper-assisted collinear SPIDER: fast and simple broadband pulse compression in nonlinear microscopy," *Journal of the Optical Society of America B* **24**(5), pp. 1091–1100, 2007.

[50] J. Sung, B.-C. Chen, and S.-H. Lim, "Single-beam homodyne SPIDER for multiphoton microscopy," *Optics Letters* **33**(13), pp. 1404–1406, 2008.

[51] K. C. Neuman and S. M. Block, "Optical trapping," *Review of Scientific Instruments* **75**(9), pp. 2787–2809, 2004.

[52] F. Gittes and C. F. Schmidt, "Interference model for back-focal-plane displacement detection in optical tweezers," *Optics Letters* **23**(1), pp. 7–9, 1998.

[53] W. M. Lee, P. J. Reece, R. F. Marchington, N. K. Metzger, and K. Dholakia, "Construction and calibration of an optical trap on a fluorescence optical microscope," *Nature Protocols* **2**, pp. 3226–3238, 2007.

[54] I. M. Tolic-Norrelykke, K. Berg-Sorensen, and H. Flyvbjerg, "MatLab program for precision calibration of optical tweezers," *Computer Physics Communications* **159**(3), pp. 225–240, 2004.

[55] P. M. Hansen, I. M. Tolic-Norrelykke, H. Flyvbjerg, and K. Berg-Sorensen, "tweezercalib 2.1: Faster version of MatLab package for precise calibration of optical tweezers," *Computer Physics Communications* **175**(8), pp. 572–573, 2006.

[56] A. Ashkin, "Acceleration and trapping of particles by radiation pressure," *Physics Review Letters* **24**, pp. 156–159, Jan 1970.

[57] A. Ashkin and J. M. Dziedzic, "Optical levitation by radiation pressure," *Applied Physics Letters* **19**(8), pp. 283–285, 1971.

[58] K. Dholakia, G. Spalding, and M. MacDonald, "Optical tweezers: the next generation," *Physics World* **15**, pp. 31–35, 2002.

[59] A. Ashkin, "Forces of a single-beam gradient laser trap on a dielectric sphere in the ray optics regime," *Biophys. J.* **61**(2), pp. 569–582, 1992.

[60] K. Dholakia, H. Little, C. T. A. Brown, B. Agate, D. McGloin, L. Paterson, and W. Sibbett, "Imaging in optical micromanipulation using two-photon excitation," *New Journal of Physics* **6**, 2004.

[61] N. K. Metzger, E. M. Wright, W. Sibbett, and K. Dholakia, "Visualization of optical binding of microparticles using a femtosecond fiber optical trap," *Optics Express* **14**(8), pp. 3677–3687, 2006.

[62] D. Morrish, X. S. Gan, and M. Gu, "Morphology-dependent resonance induced by two-photon excitation in a micro-sphere trapped by a femtosecond pulsed laser," *Optics Express* **12**(18), pp. 4198–4202, 2004.

[63] S. Kuriakose, D. Morrish, X. Gan, J. W. M. Chon, K. Dholakia, and M. Gu, "Near-field optical trapping with an ultrashort pulsed laser beam," *Applied Physics Letters* **92**(8), p. 081108, 2008.

[64] K. König, "Robert feulgen prize lecture. laser tweezers and multiphoton microscopes in life sciences," *Histochemistry and Cell Biology* **114**, pp. 79–92, Aug 2000.

[65] Y. Q. Jiang, Y. Matsumoto, Y. Hosokawa, H. Masuhara, and I. Oh, "Trapping and manipulation of a single micro-object in solution with femtosecond laser-induced mechanical force," *Applied Physics Letters* **90**(6), 2007.

[66] G. Westphal, R. Burgemeister, G. Friedemann, A. Wellmann, N. Wernert, V. Wollscheid, B. Becker, T. Vogt, R. Knüchel, W. Stolz, and K. Schütze, "Noncontact laser catapulting: a basic procedure for functional genomics and proteomics," *Methods in Enzymology* **356**, pp. 80–99, 2002.

[67] K. Inaba, K. Imaizumi, K. Katayama, M. Ichimiya, M. Ashida, T. Iida, H. Ishihara, and T. Itoh, "Optical manipulation of CuCl nanoparticles under an excitonic resonance condition in superfluid helium," *Physica Status Solidi B-Basic Solid State Physics* **243**(14), pp. 3829–3833, 2006.

[68] J. L. Deng, Q. Wei, Y. Z. Wang, and Y. Q. Li, "Numerical modeling of optical levitation and trapping of the "stuck" particles with a pulsed optical tweezers," *Optics Express* **13**(10), pp. 3673–3680, 2005.

[69] A. A. Ambardekar and Y. Q. Li, "Optical levitation and manipulation of stuck particles with pulsed optical tweezers," *Optics Letters* **30**(14), pp. 1797–1799, 2005.

[70] L. Y. Pan, A. Ishikawa, and N. Tamai, "Detection of optical trapping of CdTe quantum dots by two-photon-induced luminescence," *Physical Review B* **75**(16), 2007.

[71] L. G. Wang and C. L. Zhao, "Dynamic radiation force of a pulsed Gaussian beam acting on a Rayleigh dielectric sphere," *Optics Express* **15**(17), pp. 10615–10621, 2007.

[72] J. D. Jackson, *Classical Electrodynamics*, Wiley, 1998.

[73] S. Stallinga, "Radiation force on a fabry-perot slab immersed in a dielectric," *Optics Express* **14**(3), pp. 1286–1295, 2006.

[74] J. Shane, M. Mazilu, W. M. Lee, and K. Dholakia, "Optical trapping using ultrashort 12.9fs pulses," *Optical Trapping and Optical Micromanipulation V* **7038**(1), p. 70380Y, 2008.

[75] K. Svoboda and S. Block, "Biological applications of optical forces," *Annual Reviews in Biophysics and Biomolecular Structure* **23**(1), pp. 247–285, 1994.

[76] M. Comstock, V. Lozovoy, I. Pastirk, and M. Dantus, "Multiphoton Intrapulse Interference 6; binary phase shaping," *Optics Express* **12**(6), pp. 1061–1066, 2004.

[77] S.-K. Eah, W. Jhe, and Y. Arakawa, "Nearly diffraction-limited focusing of a fiber axicon microlens," *Review of Scientific Instruments* **74**(11), pp. 4969–4971, 2003.

[78] T. Cižmár, V. Kollárová, X. Tsampoula, F. Gunn-Moore, W. Sibbett, Z. Bouchal, and K. Dholakia, "Generation of multiple bessel beams for a biophotonics workstation," *Optics Express* **16**(18), pp. 14024–14035, 2008.

[79] C. Altucci, R. Bruzzese, C. de Lisio, M. Nisoli, E. Priori, S. Stagira, M. Pascolini, L. Poletto, P. Villoresi, V. Tosa, and K. Midorikawa, "Phase-matching analysis of high-order harmonics generated by truncated Bessel beams in the sub-10-fs regime," *Physical Review A* **68**(3), p. 033806, 2003.

[80] X. Tsampoula, V. Garces-Chavez, M. Comrie, D. J. Stevenson, B. Agate, C. T. A. Brown, F. Gunn-Moore, and K. Dholakia, "Femtosecond cellular transfection using a nondiffracting light beam," *Applied Physics Letters* **91**(5), 2007.

[81] J. Amako, D. Sawaki, and E. Fujii, "Microstructuring transparent materials by use of nondiffracting ultrashort pulse beams generated by diffractive optics," *Journal of the Optical Society of America B-Optical Physics* **20**(12), pp. 2562–2568, 2003.

[82] Y. Matsuoka, Y. Kizuka, and T. Inoue, "The characteristics of laser micro drilling using a Bessel beam," *Applied Physics A-Materials Science & Processing* **84**(4), pp. 423–430, 2006.

[83] R. Grunwald, M. Bock, V. Kebbel, S. Huferath, U. Neumann, G. Steinmeyer, G. Stibenz, J. L. Néron, and M. Piché, "Ultrashort-pulsed truncated polychromatic Bessel-Gauss beams," *Optics Express* **16**(2), pp. 1077–1089, 2008.

[84] R. Grunwald, U. Griebner, F. Tschirschwitz, E. T. J. Nibbering, T. Elsaesser, V. Kebbel, H.-J. Hartmann, and W. Jüptner, "Generation of femtosecond Bessel beams with microaxicon arrays," *Optics Letters* **25**(13), pp. 981–983, 2000.